International Journal of
Molecular Sciences

MDPI

Article

Brain Single-Cell Transcriptional Responses to Bexarotene-Activated RXR in an Alzheimer's Disease Model

Carolina Saibro-Girardi [1,2,†], Yi Lu [1], Nicholas F. Fitz [1], Daniel P. Gelain [2], Iliya Lefterov [1] and Radosveta Koldamova [1,*]

[1] Department of Environmental and Occupational Health, University of Pittsburgh, Pittsburgh, PA 15261, USA; cag237@pitt.edu or carolina.girardi@ufcspa.edu.br (C.S.-G.); yil197@pitt.edu (Y.L.)
[2] Cell and Molecular Biology Graduate Program, Biotechnology Center, Federal University of Rio Grande do Sul, Porto Alegre 91501-970, RS, Brazil
* Correspondence: radak@pitt.edu
† Current address: Department of Basic Health Sciences, Federal University of Health Sciences of Porto Alegre, Porto Alegre 90050-170, RS, Brazil.

Abstract

Pharmacological activation of brain Retinoid X Receptors (RXRs) enhances cognition and facilitates amyloid-beta (Aβ) clearance in Alzheimer's disease (AD) mouse models, partly by upregulating apolipoprotein E (*Apoe*), a major AD genetic risk factor. However, the specific cellular contributions to these effects are unclear. Here, we used single-cell transcriptomic profiling to investigate cell subpopulation-specific responses to bexarotene, an RXR agonist, in APP/PS1 mice. Our analysis revealed that bexarotene activated cholesterol biosynthesis and lipid metabolism transcriptional programs in homeostatic astrocytes and oligodendrocytes. Astrocytes also upregulated neurodevelopmental genes, while oligodendrocytes and endothelial cells showed enhanced protein folding and cellular growth pathways. Bexarotene further modulated immune responses, promoting Aβ-responsive signatures in disease-associated microglia and reactive astrocytes while dampening pro-inflammatory responses in homeostatic microglia and endothelial cells. Furthermore, *Apoe* expression was significantly elevated across multiple cell types, especially in microglia and oligodendrocytes. Cell–cell communication analysis highlighted increased astrocyte-centered signaling, with APOE-driven pathways emerging as a prominent mediator. These findings clarify the molecular complexity of RXR-mediated regulation, revealing the cellular origins of bexarotene's known effects as well as novel, cell-type-specific responses. This study provides mechanistic insights into RXR-targeted interventions and supports APOE-associated pathways as promising therapeutic targets in AD.

Keywords: Alzheimer's disease; APP/PS1 mice; RXR; bexarotene; APOE; scRNA-seq

Academic Editors: Andrea Latini and Valerio Caputo

Received: 20 February 2026
Revised: 3 March 2026
Accepted: 4 March 2026
Published: 6 March 2026

1. Introduction

Alzheimer's disease (AD) is the leading cause of dementia, accounting for up to 80% of all cases [1]. It is characterized by extracellular β-amyloid (Aβ) plaques, Tau-containing intracellular neurofibrillary tangles, and neuroinflammation. Late-onset AD is believed to result from complex interactions between environmental and genetic risk factors, with *APOE* variants encoding apolipoprotein E (APOE) being the primary genetic contributor. APOE impacts amyloid deposition by interacting with Aβ, regulating its aggregation, clearance, and cell degradation in an isoform-dependent manner [2]. Additionally, APOE-containing lipoproteins transport cholesterol from glial to neuronal cells [3]. Beyond APOE

dysfunction, AD involves metabolic disruptions [4], increased unfolded protein response (UPR) linked to Tau and Aβ [5], vascular dysfunctions [6,7], brain demyelination triggered by neuronal cell death [8], and impaired adult neurogenesis [9].

Targeting brain nuclear receptors (NR) has shown promise in AD mouse models [10]. NR are ligand-activated transcription factors regulating gene expression involved in energy metabolism, development, cell growth, and survival in response to lipophilic molecules. Retinoid X Receptors (RXR) are NR that act as obligatory heterodimerization partners for various family members, including Retinoic Acid Receptors (RAR), thyroid hormone receptors, Liver X Receptors (LXR), and Peroxisome Proliferator-Activated Receptors (PPAR). RXR activation acts primarily through permissive dimers, where RXR agonists alone can drive transcriptional activity. In the brain, the permissive RXR partners mainly include LXR, linked to oxysterol responses, and PPAR, related to fatty acid (FA) responses, along with orphan NR. While endogenous RXR ligands, such as 9-cis-retinoic acid (9-cis-RA) and 9-cis-13,14-dihydroretinoic acid, have been identified, the physiological roles of RXR activation remain debated. Nevertheless, synthetic RXR-selective agonists have been developed, leading to numerous studies on their regulatory influence over complex gene networks [11].

Bexarotene, a synthetic RXR-selective agonist and an FDA-approved drug for cutaneous T-cell lymphoma, has been extensively studied for its AD potential. Studies, including our own, have shown that it significantly improves cognition and memory in mice carrying familial AD mutations [12–15] and AD-associated APOE isoforms [16,17]. Bexarotene also facilitates soluble Aβ clearance in APP/PS1dE9 mice (APP/PS1), which express APP and PS1 mutations, though its effect on plaque load remains controversial [14,15,17]. The neuroprotective effects of RXR activation in AD are linked to APOE biology: increased APOE gene or protein expression has been observed following short-term bexarotene treatment in the brains of APP/PS1 [14,18,19] and APOE3 mice [20], with similar effects reported after long-term treatment in 3xTg-AD mice [13]. Furthermore, RXR-regulated networks control brain metabolism by mediating mitochondrial biogenesis, lipid biosynthesis, and efflux [21,22].

Numerous studies also connect bexarotene treatment to the regulation of brain immune responses. We demonstrated that bexarotene-treated APP/PS1 mice exhibit activated gene expression associated with disease-associated microglia, alongside an increased ability for Aβ phagocytosis in vitro [18]. Concurrently, bexarotene promotes an anti-inflammatory cytokine profile and reduces pro-inflammatory markers in AD and other neuroinflammatory models [12,13,19,23–26]. Furthermore, we have further demonstrated that it regulates neurodevelopmental gene expression programs, promoting neuronal differentiation in embryonic stem cells, enhancing proliferation in neurogenic sites of the APOE4 mouse brain, and maintaining dendritic complexity in primary neurons exposed to Aβ [27,28]. In adult neural stem cells, bexarotene increased self-renewal, improved late neuronal differentiation, and promoted astrogenesis [29]. Lastly, RXR-controlled networks also foster myelination in AD [30,31]. However, these processes involve multicellular responses in the brain, and the mechanisms by which RXR activation affects different brain cell types remain unclear.

Therefore, our goal was to investigate the transcriptional events triggered by bexarotene in discrete brain cell populations. Using APP/PS1 model, double-transgenic mice expressing APP/PS1dE9 mutations, we employed single-cell transcriptomics to achieve cell-level resolution in vivo. Our findings demonstrate that bexarotene-driven RXR activation promotes *Apoe* expression and regulates lipid metabolism, neurodevelopment, protein folding, and immune responses in a cell subtype-specific manner.

2. Results

2.1. Single-Cell Transcriptomics of APP/PS1 Mouse Brains Identify Glial, Neuronal, and Vascular Cell Populations

Previous studies have explored the biochemical and behavioral effects of bexarotene in APP/PS1 mice displaying an established physiopathology, showing cognitive recovery, increased APOE levels, and neuroinflammatory modulation [14,15,17–19]. To obtain further insight into the cell-specific response underlying brain RXR activation, we treated five-month-old APP/PS1 mice with bexarotene (N = 4, two male, two female) or vehicle (N = 4, two male, two female) through oral gavage for ten consecutive days, following previous studies [17,18]. At this stage, APP/PS1 mice exhibit early AD pathophysiology [32]. The dissected cortical plate was enzymatically dissociated to generate cell suspensions for the single-cell RNA sequencing (scRNA-seq) workflow of the bexarotene-treated group (Bexa) and the vehicle-treated group (Ctrl) (Figure 1A).

After cell quality control and filtering (Figure S1A,B), transcriptional data from 37,634 high-quality cells were preprocessed [33]. Dimensional reduction followed by clustering analysis [34] identified 19 discrete cell populations across all samples (Figure 1B). Cluster differential expression analysis (Figure S1C) and evaluation cell-type-specific gene sets (Figure S1D) enabled precise cell population identification (Figure 1C).

Figure 1D illustrates the expression levels of top marker genes for each cluster, and Figure 1E highlights key cell-type-specific genes used for annotation. The glial population included astrocytes expressing *Cldn10*, *Ntsr2*, and *Aqp4* (clusters 1, 5, and 7) and microglia expressing *Csf1r*, *Selplg*, and *Tmem119* (clusters 3, 6, and 9). The oligodendrocyte lineage featuring *Olig1* expression included mature oligodendrocytes (cluster 2) expressing *St18* and *Mag* markers of myelinating cells and immature cells (cluster 10) expressing *Tnr* and *Pdgfra*. The dataset also included brain blood vessel cells: endothelial cells (EC) expressing *Flt1* and *Cldn5* (clusters 0 and 11) and mural cells expressing *Vtn* and *Rgs5* (clusters 4 and 16). Neurons accounted for approximately 6% of the dataset, with clusters 8 and 14 encompassing a heterogeneous neuronal population. Minor brain cell populations included perivascular/parenchymal macrophages expressing *Ms4a7* and *Mrc1* (cluster 12) and choroid plexus epithelial and ependymal cells (cluster 13) expressing *Prlr* and *Tmem212*, respectively (Figures 1D,E and S1D). Clusters 13, 16, 17, and 18 comprised mixed cell populations or doublets (Figure S1D). Comparison between Ctrl and Bexa datasets showed similar cell quality control metrics (Figure S1B), with merging UMAP plots and comparable cell type distributions, despite a higher number of sampled cells in Bexa (Figure 1F,G). Male- and female-derived cells similarly displayed merging UMAP plots (Figure S1E).

2.2. Bexarotene Activates Lipid Biosynthesis and Brain Development Gene Expression in Homeostatic Astrocytes

Astrocytes represented the largest cell population in the APP/PS1 mouse brain libraries. To focus on astrocyte-specific transcriptional changes, we isolated the astrocyte clusters (1, 5, and 7), reprocessed the data, and filtered out cells expressing unspecific genes. This yielded 10,155 high-quality astrocytes across Ctrl and Bexa groups. Re-clustering identified three discrete subpopulations (Figure 2A). Astro0 exhibited high expression of genes linked to astrocyte cell adhesion (*Lsamp*), as well as genes linked to brain development, synaptic transmission, and axon guidance, resembling homeostatic astrocytes [35] (Figures 2B and S2A). Astro1 was enriched for *Aldoc* (Aldolase C) and other genes associated with metabolic processes and redox homeostasis, indicative of astrocyte reactivity [36]. Astro2 selectively expressed *Crym* (Crystallin) alongside high expression of other proliferation-associated genes, suggesting population-encompassing proliferative astro-

cytes (Figures 2B and S2A). Astrocyte subcluster distribution was similar between Ctrl and Bexa, as well as male and female mice (Figure S2B).

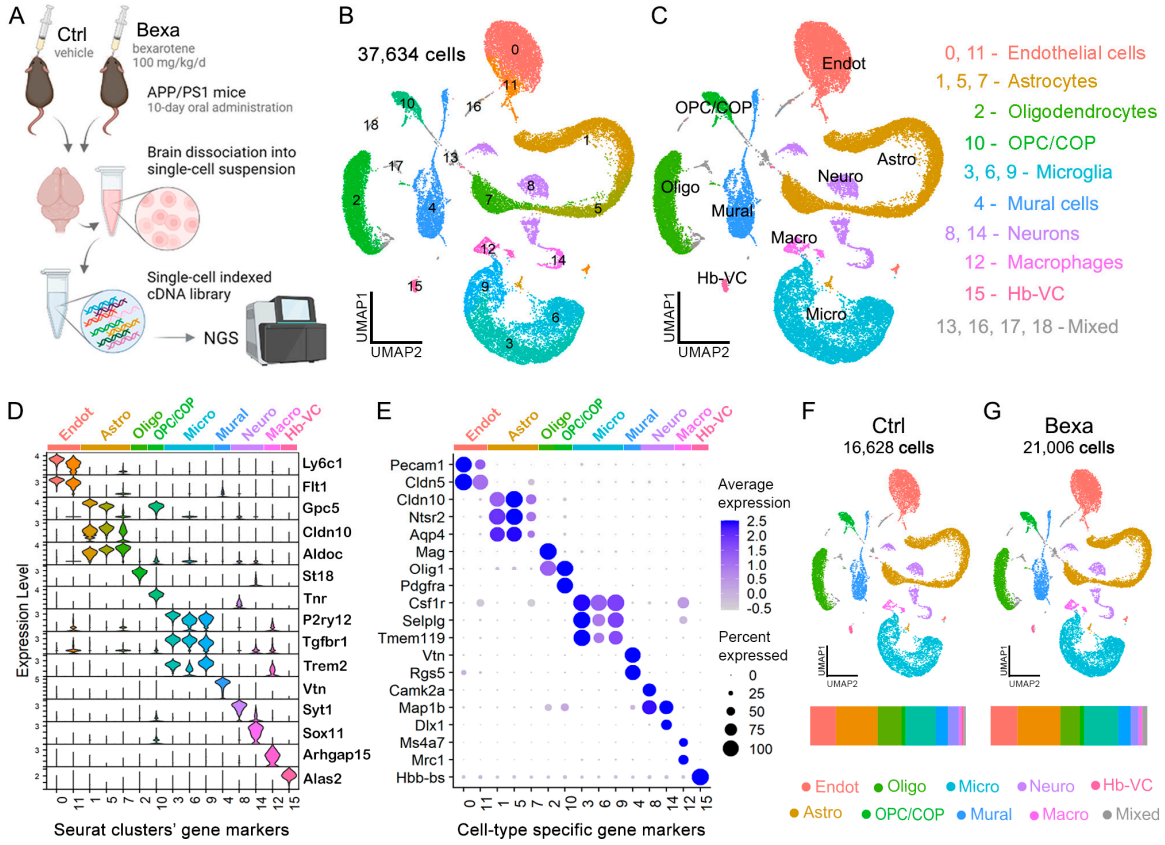

Figure 1. scRNA-seq data of bexarotene-treated APP/PS1 mouse brains. (**A**) Study design and scRNA-seq workflow. APP/PS1 mice (5 mo., male/female) were treated with bexarotene (Bexa, 100 mg/kg/d) or vehicle (Ctrl, corn oil with DMSO 1%) for 10 days through oral administration. Next, the mouse brains were dissected and dissociated into cell suspensions used for a single-cell RNA-seq workflow using the 10X Chromium platform and next-generation sequencing (NGS). (**B**) UMAP dimensional reduction of 37,634 high-quality cells detected. (**C**) UMAP plots grouped by cell type, identified after clusters' DE analysis. We identified astrocytes (Astro, 10,155 cells), microglia (Micro, 7820), oligodendrocyte lineage (Oligo and OPC/COP, 6159), neuronal lineage (Neuro, 2296), blood vessel cells (Endot and Peric, 8421), and brain monocyte/macrophages (Macro, 636). Clusters 13, 16, 17, and 18 comprised mixed cell populations or doublets. (**D**) Expression level of clusters' gene markers and (**E**) average expression plus the percent of cells expressing examples of cell type markers. (**F**,**G**) UMAP plots grouped by cell type, split by group treatment, with Ctrl (16,627 cells) and Bexa groups (21,006 cells), respectively. The bars at the bottom show the distribution of cell type populations sampled for each respective group.

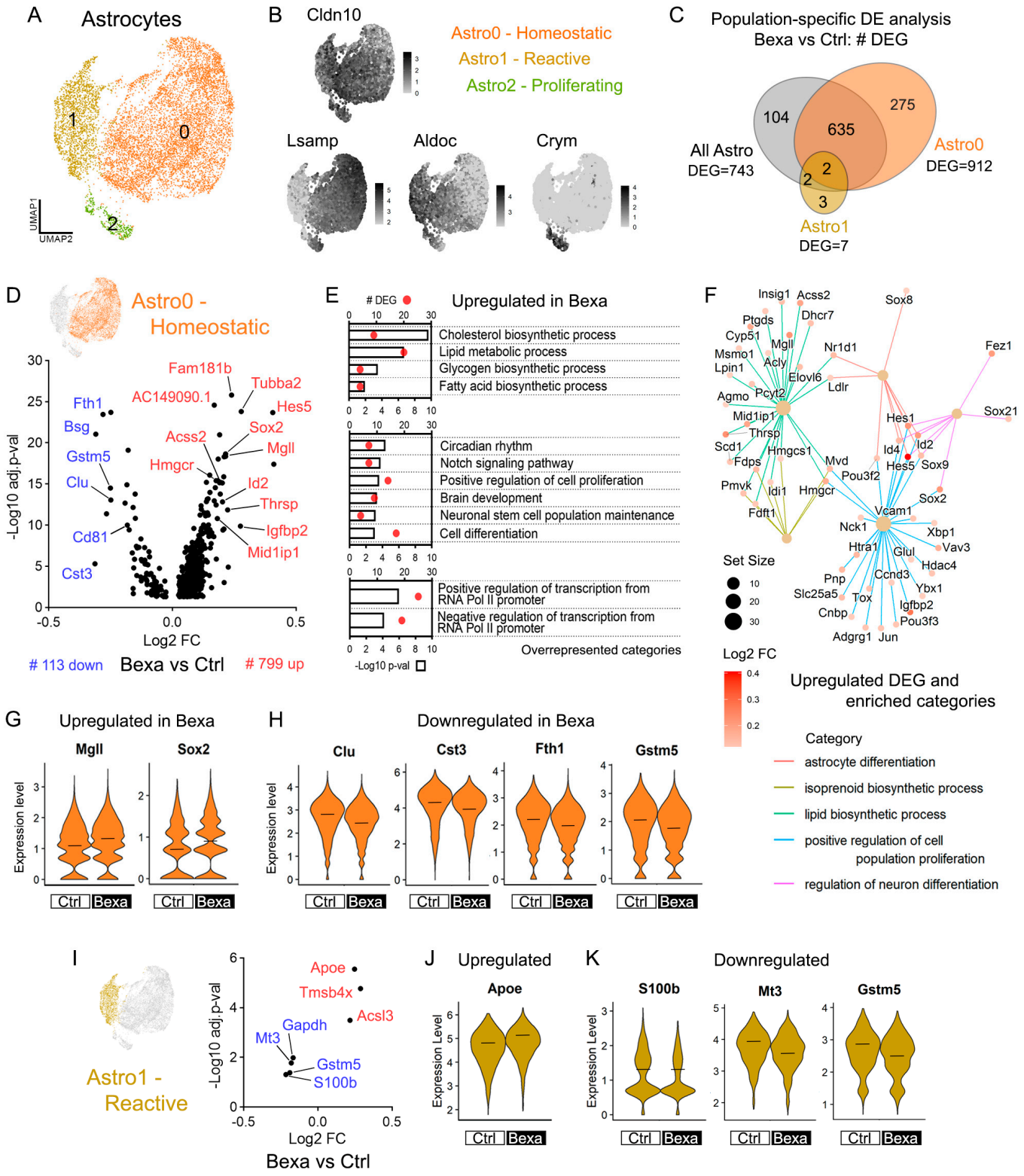

Figure 2. Bexarotene-mediated transcriptional responses in homeostatic and reactive astrocytes. (**A**) UMAP plot of the 10,002 astrocytes revealing 3 subclusters: Astro0—homeostatic; Astro1—reactive; and Astro3—proliferative. (**B**) Feature plots of subclusters' gene markers: Cldn10 (all Astro), Lsamp (Astro0), Aldoc (Astro1), and Crym (Astro3). Scales indicate the expression level. (**C**) Venn diagram of Bexa vs. Ctrl DE analysis with total, exclusive, and shared DEG numbers in astrocyte populations. Tests considered Astro0, Astro1, or all astrocyte cells. DEGs display adj.*p*-value < 0.05 and are expressed in >20% of Ctrl or Bexa cells. (**D**) Volcano plot of 799 upregulated and 113 downregulated

DEGs (#) in Bexa vs. Ctrl comparison within Astro0—homeostatic astrocytes. (**E**) Overrepresented GO terms (biological process) associated with the list of log2FC > 0.1 upregulated genes in the Bexa group within Astro0. Bars indicate −log10 *p*-value, and dots indicate DEG count. (**F**) Category netplot of upregulated DEGs in the Bexa group within Astro0, connected with the categories found in GSEA analysis. Scales indicate the gene set size and DEG log2FC. (**G**,**H**) Expression level of upregulated and downregulated genes, respectively, within Astro0 cells. (**I**) Volcano plot of DEGs in Bexa vs. Ctrl comparison within Astro1—reactive astrocytes. (**J**,**K**) Expression level of upregulated and downregulated genes, respectively, within Astro1 cells. Crossbars indicate mean values, and the expression levels are displayed as SCTransform-corrected UMI counts. Sample size: Bexa = 4305, Ctrl = 3280 (Astro0); Bexa = 1154, Ctrl = 879 (Astro1).

Next, we performed Bexa vs. Ctrl differential expression (DE) analysis considering either the total astrocyte population or selective subclusters. Figure 2C shows that most differentially expressed genes (DEG) were concentrated in Astro0-Homeostatic astrocytes. DE analysis within Astro0-Homeostatic cells identified 912 DEGs, with 799 being up- and 113 being downregulated (Figure 2D and Table S1). Numerous genes involved in lipid metabolism were upregulated. The enriched GO term cholesterol biosynthesis process included coding genes for enzymes in the mevalonate pathway (*Hmgcr*, *Pmvk*, *Mvd*, *Fdps*, *Fdft1*, *Cyp51*, *Msmo1*, *Dhcr7*) (Figures 2D,E and S2C), which is controlled by both LXR/RXR and PPAR/RXR dimers [37]. Likewise, the terpenoid backbone biosynthesis and steroid biosynthesis pathways were enriched (Figure S2D,E). For instance, the upregulated *Hmgcr* (Figure S2D) encodes the rate-limiting enzyme HMG-CoA reductase for cholesterol synthesis. The upregulation of lipid metabolic processes also included lipogenic genes (*Acss2*, *Mid1lip1*, *Thrsp*) and genes linked to the FA biosynthetic process (*Mgll*, *Elovl6*, *Scd1*, *Ptgds*) (Figures 2D–F and S2C). The lipase-coding *Mgll* (Figure 2G) converts monoacylglycerols into free FA and glycerol, while the LXR/RXR target genes *Elovl6* (ELOVL Fatty Acid Elongase 6) and *Scd1* (Stearoyl-CoA Desaturase 1) are crucial for FA elongation [38]. These findings indicate that bexarotene stimulates cholesterol and FA biosynthesis in homeostatic astrocytes, which correlates with the transcriptional changes to vital processes for brain homeostasis, learning, and cognition [3].

Genes involved in brain development were also activated within Astro0 (Figure 2D–F). Examples include transcription factor (TF)-coding genes such as *Sox2* (Figure 2G), *Sox9*, and *Sox21* from the SRY-box family, as well as *Hes5* (Figure S2C) and *Hes1* from the Hes family. The genes *Id2* (Figure S2C) and *Id4*, from the inhibitors of the DNA-binding family, were also upregulated. These families of genes play key roles in the enriched terms' cell differentiation, neuronal stem cell population maintenance, positive regulation of cell proliferation, notch signaling pathway, and circadian rhythm (Figure 2E). These TFs participate in astrocyte differentiation and the regulation of neuronal differentiation (Figure 2F) and play fundamental roles in the stemness and differentiation of adult neural progenitor cells. The upregulated *AC149090.1*, encoding a phosphatidylserine decarboxylase, is recognized as an aging clock in neural stem cells (NSC), involved in both neurodevelopment and metabolism [39]. Given the transcriptional similarities between astrocytes and NSC [40], Astro0 possibly contains a mixture of mature astrocytes and immature glial cells, including adult stem cells. Furthermore, the numerous DEGs linked with positive regulation of cell proliferation (*Igfbp2*, *Ccnd3*, *Sox2*, *Hes5*, *Id4*, *Jun*) indicate stimuli promoting the cell growth of non-reactive astroglia (Figure 2F). These findings align with our previous studies linking RXR activation with brain regeneration and the differentiation of both neurons and glial cells [27–29]. Additionally, several TFs were upregulated, as illustrated by the terms positive and negative regulation of transcription from the RNA Pol II promoter (Figure 2E). It indicates extensive secondary transcriptional events in Bexa homeostatic astrocytes, as

revealed by the enrichment of transcription regulation and chromatin remodeling using multiome analysis in this cell type [41].

The top downregulated genes in Bexa included *Clu* (Clusterin), *Cst3* (Cystatin C), *Fth1* (Ferritin heavy chain 1), and *Cd81* (Tetraspanin) (Figure 2D,H), all of which are associated with the AD-associated astrocyte phenotype [35]. The downregulation of the glutathione S-transferase coding gene *Gstm5* (Figure 2H) was observed in both Astro0 and Astro1. *Fth1* and *Gstm5* are important for oxidative stress responses, along with other downregulated genes (*Scara3*, *Cox4l1*, *Cox6c*, *Mgst1*, *Txnip*, *Prnp*) (Table S1). *Cst3*, *Clu*, and *Cd81* are involved in astrocyte immunoreactivity and cell proliferation, with Cystatin C and Clusterin being well-known players in Aβ trafficking and plaque-associated responses (Figure 2G) [35,42]. Conversely, *Abca1* (ATP-binding cassette transporter A1), an LXR target gene linked to lipid transport, was also downregulated, though to a lesser extent (Table S1). Overall, our findings indicate that neuroinflammatory, stress-related, and AD-associated features are reduced in homeostatic astrocytes following bexarotene treatment.

2.3. Reactive Astrocytes Display Upregulated Apoe and Suppressed Stress-Related Genes Under RXR Activation

Reactive astroglia refers to the astrocyte population that undergoes cellular programs in response to a pathological context, leading to a range of reactive phenotypes [36]. Among them, an AD-unique disease-associated astrocyte population has been reported, expressing high levels of genes related to amyloid metabolism and clearance [35]. Within the reactive astrocytes recognized as Astro1 in the APPS/PS1 model, we identified fewer Bexa-associated DEGs compared to Astro0-Homeostatic (Figure 2C and Table S1). Astro1-Reactive showed seven DEGs in Bexa vs. Ctrl (Figure 2I), five exclusive to Astro1, including the AD-linked *Apoe* (Figure 2J), *Acsl3* (Acyl-CoA Synthetase Long-Chain Family Member 3) involved in lipid biosynthesis and beta-oxidation, and *Tmsb4x* (Thymosin beta-4) linked to cytoskeleton organization. *Apoe* expression is a fundamental feature of astroglia, and in AD-associated astrocytes, it is also linked to Aβ reactivity [43,44]. Its upregulation in Bexa Astro1 thus suggests increased Aβ reactivity in reactive astrocytes following the treatment.

Conversely, *S100b* (S100 Calcium-Binding Protein B), *Mt3* (Metallothionein 3), and *Gstm5* are also involved in astrocyte reactivity but were downregulated in Astro1 (Figure 2K). S100B, also downregulated in Astro0, is recognized as a protein expressed and released by astrocytes under brain injury, acting as a damage-associated molecular pattern [45]. Together with the roles of *Mt3* and *Gstm5* activation in oxidative stress, our findings thus indicate reduced stress responses in reactive astrocytes of bexarotene-treated APP/PS1 mice.

2.4. Bexarotene Activates Microglial Apoe and Differentially Modulates Immune Reactivity-Associated Genes in Homeostatic and DAM Populations

Next, we analyzed microglial cell populations in the APP/PS1 mouse brain. Clusters 3, 6, and 9 were analyzed as a subset, yielding a final 7567 high-quality cells. Re-clustering identified three distinct populations: Micro0-DAM1, Micro1-Homeostatic, and Micro2-DAM2 (Figure 3A). Disease-associated microglia (DAM) are a subset of brain immune cells found at neurodegeneration sites, playing protective roles through the activation of phagocytic, lysosomal, and lipid metabolism pathways [46]. Cluster Micro1-Homeo displayed gene expression associated with homeostatic microglial functions, such as *Malat*, *Nav3*, and *Tanc2* (Figures 3B and S3A). By contrast, both Micro0 and Micro2 displayed high levels of classical DAM genes like *Tpt1*, *Tyrobp*, *Trem2*, and *Apoe*, but the 511 cells of Micro2-DAM2 selectively expressed *Cst7*, which is spatially correlated with amyloid plaques [47,48] (Figures 3B and S3A,B). Micro0-DAM1 also expressed relatively high levels of *Cst3*, *Aif1*, and *C1q* family of complement genes (Figure S3A). Comparing cluster

distributions between treatment groups and animal sex revealed equivalent proportions: 43% homeostatic (Micro1) and 57% DAM (Micro0 & Micro2) (Figure S3C).

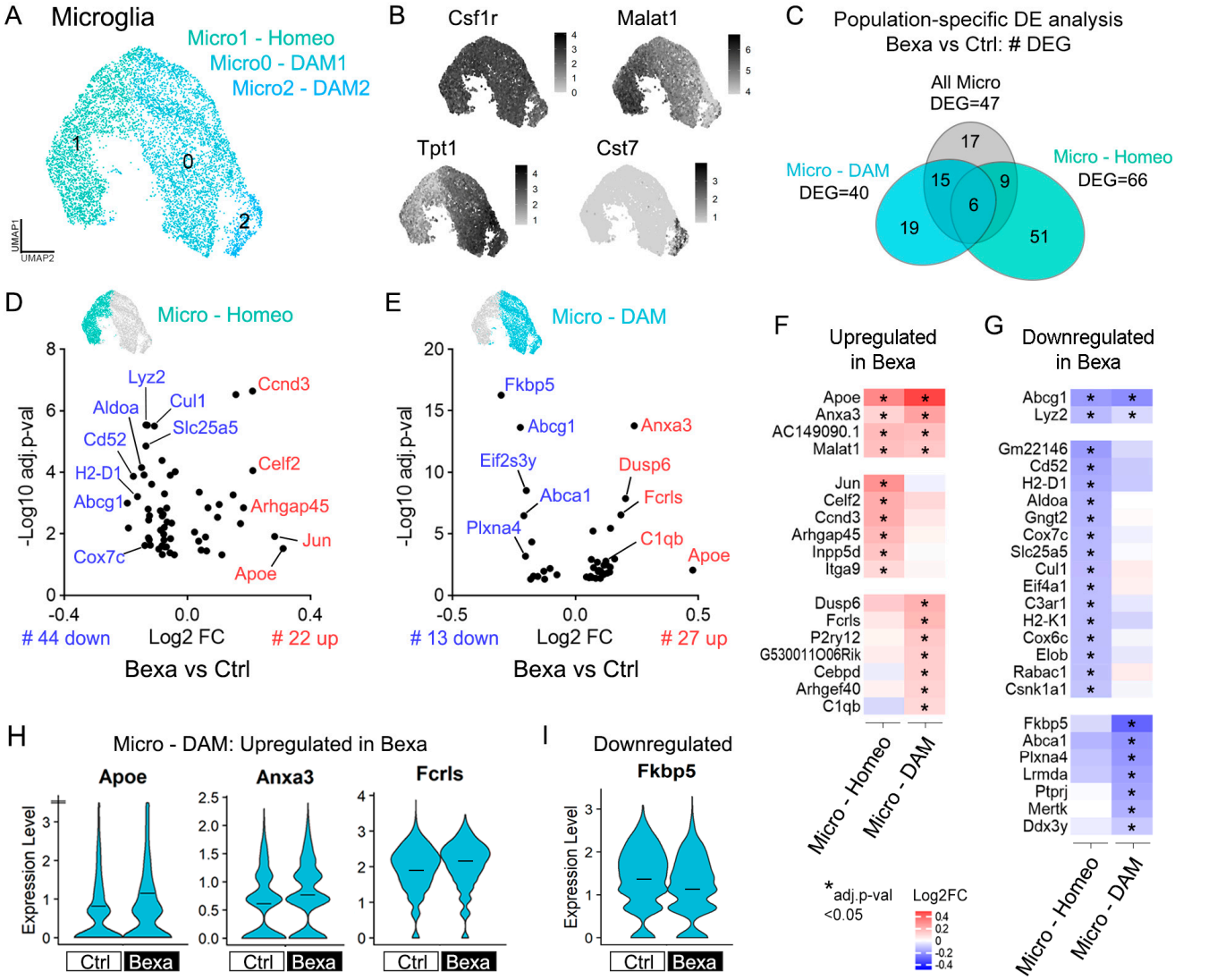

Figure 3. DAM and homeostatic microglia-specific transcriptional responses in APP/PS1 mice treated with bexarotene. (**A**) UMAP plot of the 7106 cells showing Micro0, Micro1, and Micro2 subclusters. (**B**) Feature plots of subclusters' gene markers: Csf1r (all Micro), Malat1 (Micro1, homeostatic), Tpt1 (Micro0, DAM), and Cst7 (Micro1, DAM). (**C**) Venn diagram of Bexa vs. Ctrl DE analysis with total, exclusive, and shared DEG numbers in microglia populations. Tests considered the homeostatic (Micro1), DAM (Micro0 & Micro2), or all Micro populations. DEGs display adj.*p*-value < 0.05 and are expressed in >20% of Ctrl or Bexa cells. (**D**,**E**) DE analysis within Micro—Homeo and Micro—DAM, respectively. Volcano plots of 22 up- and 44 downregulated DEGs (#) within Micro—Homeo and of 27 up- and 13 downregulated DEGs (#) within Micro—DAM populations. (**F**,**G**) Heatmaps showing Bexa vs. Ctrl fold change of upregulated and downregulated DEGs, respectively, in microglia subpopulations. DEGs in both identities (top panels), in Micro—Homeo only (middle) and in Micro—DAM only (bottom). Scales indicate Bexa vs. Ctrl log2FC, and * indicates adj.*p*-value < 0.05. (**H**,**I**) Expression level of the upregulated and downregulated genes, respectively, within the Micro—DAM population. Crossbars indicate mean values. Expression levels are displayed as SCTransform-corrected UMI counts. Sample size: Bexa = 2396, Ctrl = 1662 (DAM); Bexa = 1861, Ctrl = 1187 (Homeo).

We merged Micro0 and Micro2 into a single DAM cluster and conducted Bexa vs. Ctrl DE analysis across the entire microglial population, Micro-Homeo, and Micro-DAM.

Compared to astrocytes, microglia exhibited fewer DEGs: 66 genes in Homeo, 40 genes in DAM, and 47 genes when all microglia were considered (Figure 3C and Table S1). Notably, the gene sets affected in Micro-Homeo and Micro-DAM were largely distinct (Figure 3C–E). Figures 2F and 2G, respectively, compare the gene sets upregulated and downregulated in Bexa in both microglial subpopulations.

Within the DAM population (Micro-DAM), Bexa exhibited the activation of 27 genes and the downregulation of 13 (Figure 3E). *Apoe* and the microglial gene *Anxa3* (Annexin 3) were the top Bexa-induced genes within this population, which were also upregulated in Micro-Homeo but to a lesser extent (Figure 3F). *Apoe* (Figure 3H) is crucial for DAM phenotype acquisition, acting also via the APOE/TREM2 axis to direct lipoprotein-ligated Aβ for degradation by microglia [46]. *Anxa3* (Annexin 3) (Figure 3H) regulates cell growth in immune cells and is found upregulated in activated microglia [49]. In Micro-DAM, upregulated genes were also connected to the activation/control of MAPK signaling pathways (*Anxa3*, *Dusp6*, *Fcrls*) (Figure 3E,F). For instance, *Fcrls* (Figure 3H), an Fc receptor family member, interacts with opsonized immune complexes, driving their phagocytosis. The complement gene C1qb was also upregulated in Bexa within DAM cells (Figure 3E,F). These results indicate that bexarotene enhances immune responses and Aβ reactivity in DAM of APP/PS1 mice. A similar response has been reported in macrophages [18,26], though we did not detect DEGs in cluster 12 containing macrophages.

The top downregulated gene in Micro-DAM was *Fkbp5* (Figure 3G,I), which was also described in chromatin accessibility data [41]. *Fkbp5* encodes a peptidyl-prolyl isomerase with co-chaperone activity known to promote neuroinflammation and cytotoxicity through NF-κB activation [50]. This finding thus supports the role of RXR activation in reducing neuroinflammation through LXR- and PPAR-mediated inhibition of NF-κB [37] and aligns with PPARα-induced suppression of FKBP5 in the APP/PS1 cortex [51]. Lastly, *Lyz2* and the LXR target gene *Abcg1* were downregulated within Bexa in both DAM and homeostatic microglia, while *Abca1* was specifically downregulated in Micro-DAM (Figure 3G). This indicates that Bexa-associated *Apoe* upregulation in microglia is functioning through ABCG1/ABCA1-independent immune pathways [19,52–54].

2.5. Oligodendrocytes Display Upregulated Cholesterol Synthesis and Protein Folding Gene Expression Following Bexarotene Treatment

We next analyzed the oligodendrocyte lineage subset, encompassing clusters 2 and 10. The final dataset comprised 5898 high-quality cells, primarily mature oligodendrocytes alongside a population containing oligodendrocyte precursor cells (OPC) and differentiation-committed oligodendrocyte progenitors (COP) cells (Figure S4A) [55], with similar cluster distribution between treatment groups (Figure S4B). Oligodendrocytes expressed the marker of oligodendrocyte lineage *Olig1*, along with key myelination markers such as *Plp1*, *Mbp*, and *St18* (Figures 4A,B and S4A). Bexa vs. Ctrl DE analysis revealed 141 DEGs in oligodendrocytes (Figure 4C and Table S1). Of these, 79 genes were upregulated, with *Apoe* emerging as the top activated gene (Figure 4C,D). While APOE is extensively studied in astrocytes and microglia, it also plays a critical role in oligodendrocytes, as dysfunctional APOE biology is linked to oligodendrocyte cholesterol accumulation and impaired myelin formation [56]. Another player in oligodendrocyte lipid dynamics, *Apod*, was also upregulated in Bexa (Figure 4D). APOD lipoprotein is essential for cell lipid homeostasis, controlling lipids' redox state across subcellular/extracellular locations [57]. In oligodendrocytes, APOD further contributes to the compaction of the extracellular leaflet of myelin [58].

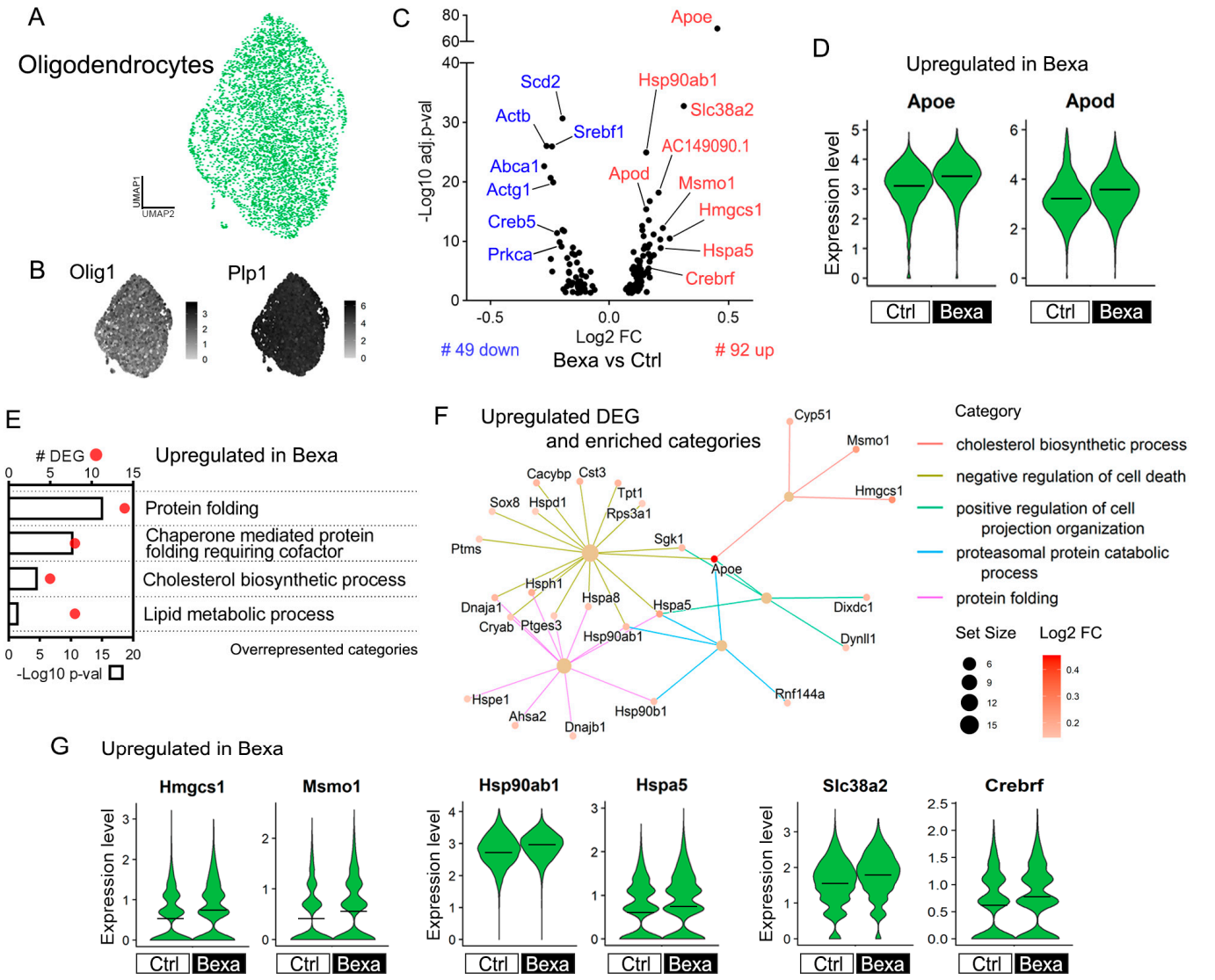

Figure 4. Oligodendrocyte gene expression responses to bexarotene treatment in APP/PS1 mice. (**A**) UMAP plot of 4987 cells with oligodendrocyte gene expression profiles. (**B**) Feature plots of gene markers: Olig1 (oligodendrocyte lineage) and Plp1 (mature oligodendrocytes). (**C**) Bexa vs. Ctrl DE analysis found 141 DEGs within oligodendrocytes, and the volcano plot displays the 79 upregulated and 45 downregulated DEGs (#). (**D**) Expression level of upregulated Apoe and Apod in Bexa oligodendrocytes. (**E**) GO terms (biological process) associated with the list of log2FC > 0.1 upregulated genes. Bars indicate −log10 *p*-value, and dots indicate DEG count. (**F**) Category netplot of upregulated DEGs in the Bexa group, connected with the categories found in GSEA analysis. Scales indicate the gene set size and DEG log2FC. (**G**) Expression level of upregulated genes linked to cholesterol biosynthetic process (Hmgcs1, Msmo1), protein folding (Hsp90ab1, Hspa5), and CREB pathway (Slc38a2, Crebrf) in Bexa within oligodendrocytes. Crossbars indicate mean values. Expression levels are displayed as SCTransform-corrected UMI counts. Sample size: Bexa = 2511, Ctrl = 2476.

The terms cholesterol biosynthetic process and lipid metabolic process were activated in Bexa oligodendrocytes, exemplified by the upregulated DEGs of the mevalonate pathway (*Hmgcs1*, *Msmo1*, *Idi1*, and *Cyp51*) (Figure 4E–G). Previous studies show that cholesterol synthesis is also essential for myelin sheath formation [59]. Among the 45 downregulated genes, we identified other fundamental controllers of lipid metabolism: *Abca1*, *Scd2* (Stearoyl-CoA Desaturase 2), and *Srebf1* (Sterol Regulatory Element-Binding Transcription Factor 1) (Figure 4C). These genes, respectively, control cholesterol efflux, fatty acid biosyn-

thesis, and lipogenesis—all consensus LXR target genes. Their downregulation suggests a suppression of key LXR-mediated responses in oligodendrocytes exposed to bexarotene.

Animal models of AD exhibit increased endoplasmic reticulum (ER) UPR stress and oxidative stress [5], which can also be regulated by RXR activation [60]. In oligodendrocytes, many Bexa-upregulated genes were linked to the term protein folding, including multiple Heat Shock Protein (HSP) family genes (*Hsp90ab1*, *Hspa5*, *Hsph1*, *Hspa1b*, *Hspa1a*) (Figure 4E–G). HSP genes were also included in the upregulated negative regulation of cell death (Figure 4F). Protein folding responses are crucial for maintaining cellular proteostasis and promoting survival under Aβ-induced ER stress. Additionally, they are closely linked to cholesterol metabolism in oligodendrocytes [56]. The treatment also affected the expression of genes involved in the CREB signaling pathways, which regulate cell growth and survival in response to stress, growth factors, and metabolic states. It activated *Crebrf* (CREB3 Regulatory Factor), as well as cAMP/PKA/CREB transcriptional targets such as *Slc38a2* and *Sgk1* (Figure 4G). In oligodendrocytes, PKA/CREB promotes myelination [61]. In parallel, *Creb5* (CREB5) and *Prkca* (PKCα kinase) were downregulated, along with cell motility-associated genes in Bexa (*Actb*, *Actg1*, Figure 4C).

Furthermore, the subset of COP/OPC cells did not show significant transcriptional changes in Bexa. However, when analyzing the entire oligodendrocyte lineage (including mature and immature cells), we identified DEGs with similar trends in COP/OPC (Figure S4C). Some of these DEGs are linked specifically to COP/OPC-associated changes in gene expression rather than mature oligodendrocytes, such as several developmental genes (*Hes5*, *Tafa1*, *Ncan*, *Ifi27*, *AC149090.1*). This reveals that bexarotene influences neurodevelopmental gene expression within the oligodendrocyte lineage, potentially affecting immature cells.

Oligodendrocyte function is also tightly linked to neuronal health, and bexarotene has been shown to regulate neuronal genes and processes in AD mouse models [27,28]. Within neuronal clusters, we identified nine distinct subpopulations, including small groups of excitatory, inhibitory, and immature neuroblasts (Figure S4D–E) [55]. However, the highly variable distribution of these subclusters across samples and the limited number of cells across subclusters (Figure S4F) prevented a robust evaluation of bexarotene's effects on neuronal populations.

2.6. Brain Endothelial Cells' Gene Responses Are Linked to Protein Folding and Vasculogenesis

AD also relates to vascular dysfunctions, including brain hypoperfusion, barrier leakiness, and other blood vessel cell vulnerabilities [6,7]. At last, single-cell transcriptomics enabled us to examine Bexa gene expression changes in mural (cluster 4) and endothelial cells (EC, clusters 0 and 11) in vivo. Analysis of mural cells comprising pericytes and vascular smooth muscle cells did not display DEGs in Bexa. In parallel, the EC subset, yielding final 5430 high-quality cells, was re-clustered into two subpopulations: EC0-Capillary/Arteriole and EC1-Venule (Figure 5A). EC0 expressed both arteriole (*Arl15*, *Mgp*, *Gkn13*) and capillary (*Ivns1abp*, *Hmcn1*) markers, with upregulated terms linked to cell cycle and migration (Figures 5B and S5A). EC1 showed upregulated venule markers (*Vwf*, *Il1r1*, *Cfh*) and other genes linked to translation and response to hypoxia (Figures 5B and S5A). Since EC1 primarily originated from a single animal (Figure S5B), we focused our analysis on EC0-Capillary/Arteriole.

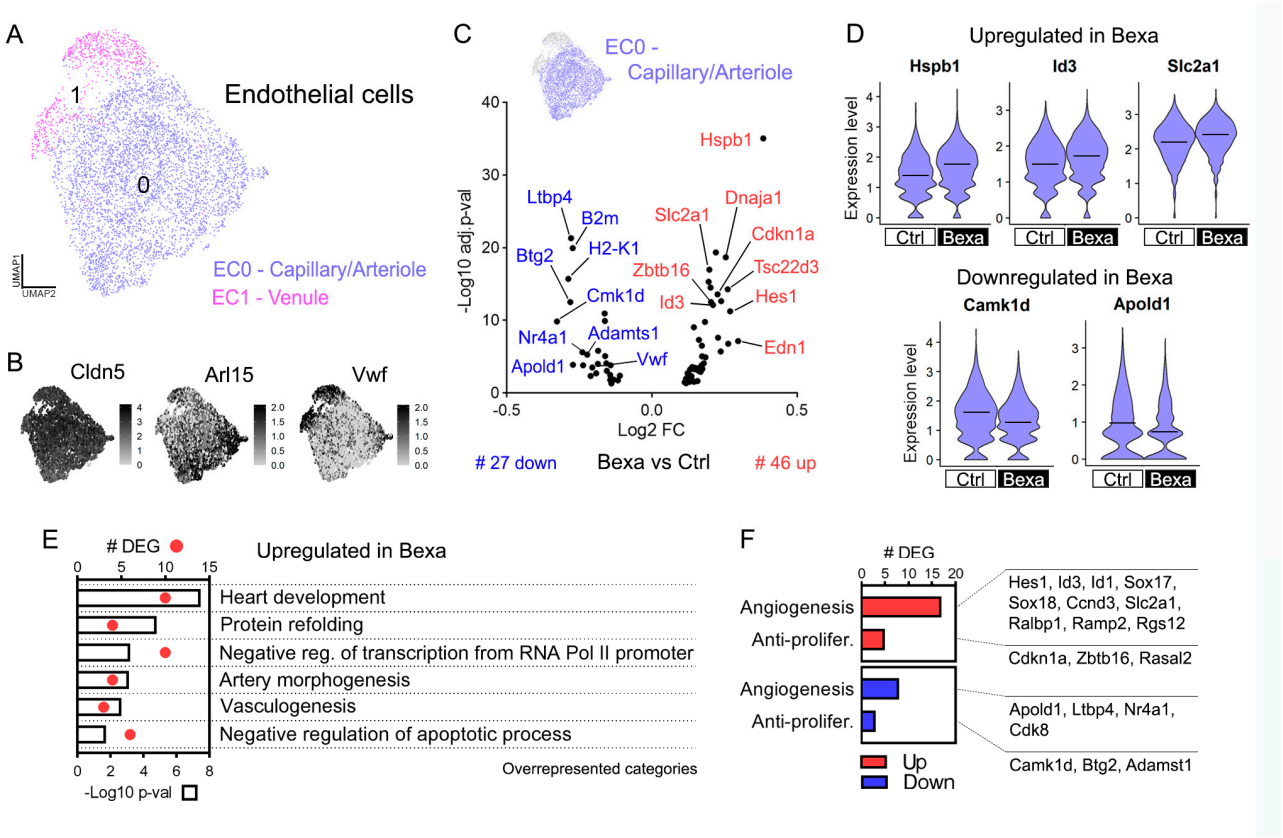

Figure 5. Brain EC molecular responses in APP/PS1 mice treated with bexarotene. (**A**) UMAP plot of the 5430 cells with EC gene expression recovered from APP/PS1 mouse brains, showing EC0—Capillary/Arteriole and EC1—Venule populations. (**B**) Feature plots of subclusters' gene markers: Cldn5 (all EC), Arl15 (EC0, arteriole), and Vwf (EC1, venule). (**C**) Bexa vs. Ctrl DE analysis found 73 DEGs within the larger capillary/arteriole brain EC (EC0) population, and the volcano plot displays the 46 upregulated and 27 downregulated DEGs (#). (**D**) Expression levels of upregulated Hspb1, Id3, and Slc2a1 in Bexa and downregulated Camk1d and Apold1 within EC0—Capillary/Arteriole. Crossbars indicate mean values, and the expression levels are displayed as SCTransform-corrected UMI counts. (**E**) Overrepresented GO categories (biological process) associated with the list of log2FC > 0.1 upregulated genes in the Bexa group within EC0. Bars indicate −log10 *p*-value, and dots indicate DEG count. (**F**) Counts for angiogenesis/EC proliferation marker genes upregulated (17) and downregulated (8) in the Bexa group and for anti-proliferative EC marker genes, both upregulated (5) and downregulated (3). Sample size: Bexa = 2968, Ctrl = 1707 (EC0).

Bexa vs. Ctrl DE analysis in EC0 identified 73 DEGs, with *Hspb1* as the top upregulated gene (Figure 5C,D and Table S1). Similarly to oligodendrocytes, the treatment increased the expression of HSPs and other protein refolding-associated genes (*Hspb1*, *Dnaja1*, *Hspa8*, *Hsp90ab1*, *Hsp90aa1*) (Figure 5E). Key upregulated GO terms included heart development and vasculogenesis, exemplified by the activation of *Hes1*, *Id3*, *Sox17*, and *Sox18* (Figure 5D,E). The regulation of these and other transcription factors was reflected in the term negative regulation of transcription from the RNA Pol II promoter. Another top upregulated gene was *Slc2a1*, encoding the blood–brain barrier (BBB)-specific transporter GLUT1, which activates glucose uptake and EC proliferation (Figure 5D). Other upregulated EC-associated genes included *Ctla2a*, *Pglyrp1*, *Edn1*, *Tbc1d4*, *Ramp2*, *Cavin2*, and *Rgs12* (Table S1).

Bexarotene-regulated genes were involved in neuroinflammation control within ECs. RXR activation upregulated *Tsc22d3* (TSC22 Domain Family Member 3), a corticosteroid-responsive anti-inflammatory transcription factor, while downregulating *B2m* and *H2-K1*

immune-associated genes in EC (Figures 5C and S5C). *Vwf* (Von Willebrand factor), which responds to vascular injury, tissue damage, and infection, was also downregulated in Bexa capillary/arteriole cells. VWF also modulates angiogenesis depending on its cellular localization [62].

Several Bexa-upregulated genes were linked to EC growth and apoptosis suppression (Figure 5E), though cell proliferation regulators showed both up- and downregulated patterns (Figure 5F). In addition to GLUT1, HES, SOX, and Id genes, Bexa-induced angiogenesis signals included *Ccnd3*, *Ralbp1*, *Rgs12*, and *Ramp2* [63,64]. Conversely, antiproliferative genes were downregulated, including *Camk1d* (CaM Kinase ID, Figure 5D), *Btg2*, and *Adamts1*. However, cell cycle inhibitors were activated (*Cdkn1a*, *Zbtb16*), and EC proliferation marks such as *Apold1* (Apolipoprotein L Domain Containing 1, Figure 5D), *Ltbp4*, *Nr4a1*, and *Cdk8* were suppressed, thus indicating simultaneous signals for control of vascular cell growth. Protein refolding responses may also influence EC proliferation. HSPB1 mediates VEGF-induced EC cytoskeleton organization, with angiogenic effects varying by its intra- or extracellular localization [65]. HSP90, encoded by the upregulated genes *Hsp90ab1* and *Hsp90aa1*, also controls EC growth by promoting cell proliferation and tube formation [66]. As shown in Figure 5F, most pro-angiogenic markers were upregulated indicating an overall stimulus for brain capillary/arteriole growth following RXR activation.

2.7. APOE-Mediated Signaling Is a Central Axis of Communication Activated by Bexarotene in Brain Cells

Apoe, a known RXR target gene, was upregulated in distinct cellular subsets following bexarotene treatment, as shown in Figure 6A. APOE interacts with multiple receptors to deliver lipids and lipoprotein-associated molecules, such as Aβ, to other cells. Activation of the APOE/TREM2 axis in reactive cells, for instance, is recognized as a key pathway for Aβ degradation and plaque compaction, triggering a downstream signaling cascade crucial for immune function [2]. To predict the impact of bexarotene on cell signaling pathways, we next conducted network analysis of cell communication. Based on the gene expression profile of ligands, receptors, and cofactors in signaling pathways provided by CellChatDB [67], we calculated and compared communication probabilities among cells acting as sources and targets of signals (Figures 6B and S6A). This analysis showed that bexarotene might strengthen the interactions between brain cells, particularly those involving astrocytes (Figures 6C and S6B–D). The number of significant interactions involving homeostatic microglia (Micro-Homeo) slightly decreased, likely reflecting the overall downregulation of gene expression induced by the treatment in this population. The APOE-mediated signaling pathway appeared among the top signaling changes induced by bexarotene in the brains of APP/PS1 mice in various cell types (Figure 6D). It showed an overall 30% increase compared to the control, with 57% of the relative information flow linked to the Bexa network (Figures 6E and S6E). The main sources of APOE were Astro-Homeo; Astro-Reactive; oligodendrocytes; and, to a lesser extent, ECs—all of which exhibited increased APOE signaling outgoing interaction strength. This pathway primarily targeted Micro-DAM and Micro-Homeo, with both showing increased incoming interaction strength, as well as Astro-Reactive in the Bexa group (Figures 6E and S6E).

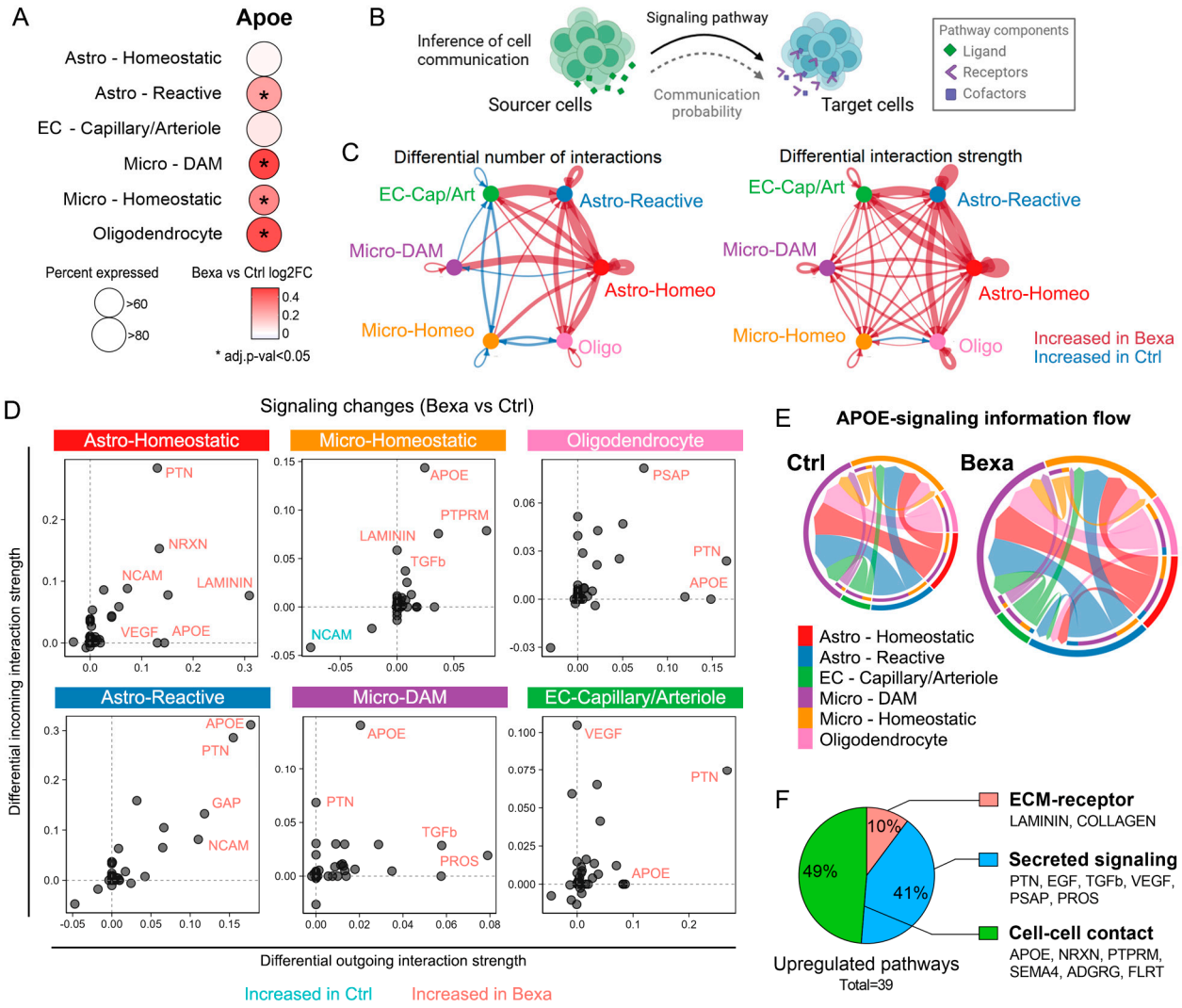

Figure 6. Cell communication inference reveals changes in APOE-mediated signaling by bexarotene. (**A**) Cell population-specific Apoe differential gene expression in response to the 10-day treatment with bexarotene in 5-month-old APP/PS1 mice. Circle size indicates the percent expressed in the Bexa group. Color scale indicates Bexa vs. Ctrl log2FC values. (**B**) CellChat was used to predict the impact of bexarotene-induced gene expression changes on the cell communication between populations. It was based on the expression profiles of gene products acting as ligands in the cell sources and receptors/cofactors in the cell targets. (**C**) Circle plots showing the overall differential number of interactions (left panel) and differential interaction strength (right panel) among distinct cell populations in Bexa compared to the Ctrl group. Red arrows indicate increased interactions in Bexa, while blue arrows indicate increased interactions in Ctrl. (**D**) Signaling changes in Bexa vs. Ctrl comparison for each cell population, showing that APOE appeared among the top axes of communication affected. The changes are expressed in terms of differential incoming (*y* axis) and outgoing (*x* axis) interaction strengths for each signaling pathway identified. (**E**) Chord diagrams showing the APOE-signaling information flow in the Ctrl and Bexa groups. The diagram size is proportional to the relative information flow. Outer bar colors represent the cell sources, and inner, thinner bar colors represent the targets. Bar size is proportional to the signal strength sent or received. Edge colors are consistent with the sources, and edge weights are proportional to the interaction strength. (**F**) CellChatDB annotation of the 39 upregulated signaling pathways strengthened by bexarotene (p-value < 0.05).

The Bexa group was associated with the upregulation of APOE and 38 other communication pathways (Figure S6E). These pathways were predominantly annotated as cell–cell contacts (49%) and secreted signalings (41%), with a smaller portion related to

extracellular matrix (ECM)–receptor contacts (10%) (Figure 6F). Cell population-specific changes show that Astro-Homeo was central to many of those changes, supported by the strong DE among these cells (Figures 6D and S6F). For example, the LAMININ pathway of ECM–receptor contact was increased between Astro-Homeo and other subsets, driven by the upregulation of *Lama3* (Laminin Subunit Alpha 3) in astrocytes (Figure S6F and Table S1). Neurexin-mediated contacts (NXRN) were upregulated between homeostatic astrocytes and other cells, associated with an increased expression of pathway components like the receptor *Dag1* (Dystroglycan 1) in Astro-Homeo (Figure S6F and Table S1).

Signaling pathways coordinated by secreted growth factors were also increased and linked to Astro-Homeo activity. PTN (Pleiotrophin) signaling, which promotes post-developmental neurotrophic and protective effects [68], had its interaction strength increased from, but particularly towards, homeostatic astrocytes, which was linked to increased levels of *Sdc4* (Syndecan 4) in these cells (Figure S6F and Table S1). Additionally, EGF (Endothelial Growth Factor) and VEGF signaling pathways were increased due to changes in the expression of their ligands in Astro-Homeo, connecting these cells with other astrocytes and EC, respectively (Figure S6F). These findings reflect the observed DE linked to neurodevelopment and angiogenesis. In contrast, analysis of signaling changes related to Astro-Reactive showed minimal correspondence, with significant changes in DE, likely due to the small number of cells in this subcluster.

In addition to APOE, pathways strengthened in the microglia populations included PTPRM (Protein Tyrosine Phosphatase Mu), SEMA4 (Semaphorin 4A), and TGFb (Transforming Growth Factor Beta), all linked to microglial cell growth and motility (Figure 6D). These changes were also connected to DE in homeostatic astrocytes, with the upregulation of Ptprm, semaphorin-coding genes, and Tgfb2 (Figure S6F and Table S1). For instance, the anti-inflammatory TGF-β cytokine is a key controller of microglia activation and AD-linked neuroinflammation [69]. These predicted changes in cell communication, centered around APOE signaling, cell growth, and immune control, reflect the biological processes affected by bexarotene across brain cell subpopulations and open new possibilities for studying RXR-regulated molecular targets and signaling pathways in AD physiopathology.

3. Discussion

Recent single-cell approaches have revealed brain cellular heterogeneity in various contexts, including AD. However, how discrete cell populations respond to potential therapeutic interventions, such as NR-targeted treatments, remains largely unknown. We investigated bexarotene's molecular impact across brain cells in APP/PS1 mice, generating a comprehensive set of DEGs. Functional predictions, based on Gene Ontology (GO) terms and cell communication pathways, revealed that bexarotene-activated RXR receptors regulate cholesterol metabolism, development, cell growth, immune reactivity, and protein folding gene sets in a cell subpopulation-specific manner. Consistent with the present findings, transposase-accessible chromatin sequencing (ATAC-seq) profiles and integrative regulatory network analysis indicated that treatment led to differentially bound TFs linked to development in astrocytes and oligodendrocytes, angiogenesis in endothelial cells, and immune activation in microglia [41].

Apoe activation was prominent in DAM and homeostatic microglia, oligodendrocytes, and reactive astrocytes of Bexa APP/PS1 mice. Our findings also show that *Apoe* upregulation is stronger in reactive and disease-associated glial cells compared to homeostatic cells. LXR and PPARγ agonists also promote this effect in APP/PS1 mice, with simultaneous activation of both receptors exerting a synergistic effect on *Apoe* activation [22,70]. Here, we identify specific brain cell subpopulations that may mediate the *Apoe* upregulation linked to RXR activation. Furthermore, we confirm the central role of APOE biology in the

molecular effects of bexarotene in the brains of APP/PS1 mice, with the APOE-mediated signaling pathway being one of the top upregulated communication axes in the Bexa group, primarily linking homeostatic and reactive glial cells.

Preclinically, bexarotene-mediated Aβ clearance and cognitive improvement require functional APOE [10], and clinical evidence confirms this link: the treatment reduced brain amyloid, increased serum Aβ, and reduced CSF Aβ selectively in APOE4 non-carrier AD subjects [71]. While this validates the RXR-APOE axis as a therapeutic target, bexarotene also induced elevated triglycerides, raising safety concerns that limit repurposing without modification [71]. Next-generation compounds targeting RXR and RXR partners aim to bypass this toxicity. For instance, a nonlipogenic LXR agonist (NLAI) retained ABCA1/APOE effects and modulated inflammation without inducing triglyceride synthesis preclinically [72], and the dual PPARδ/γ agonist T3D-959 safely slowed cognitive decline in a Phase 2 AD trial while also modulating inflammation and metabolism [73]. These compounds are promising for translating RXR-associated genomic effects into viable AD therapies, and understanding how these agents modulate pathways like lipid metabolism and inflammation in specific cell subpopulations enables intelligent design of synergistic combinations with improved efficacy and safety.

The influence on APOE lipidation status through ABCA1 and ABCG1 is also considered a key aspect of the neuroprotective effects of bexarotene in AD models [16,20]. We and others have shown the upregulation of *Abca1/Abcg1* in the brains of bexarotene-treated AD mice, controlled by LXR/RXR [13,18,74]. However, our results indicate that *Abca1/Abcg1* was either unaffected or downregulated by bexarotene in specific subpopulations, suggesting that this LXR-controlled response may vary depending on cell types and/or the physiological context. Previous studies using bulk RNA-seq of whole brains might have captured *Abca1/Abcg1* upregulation linked to cell populations not adequately represented by scRNA-seq, such as large and morphologically complex cells. Additionally, our findings reflect early-stage amyloid pathology, unlike previous studies that used older animals and different AD models. Notably, RXR-induced *Abca1* upregulation occurs only under high Aβ levels [74], indicating that RXR control over *Abca1/Abcg1* may vary according to model and disease stage. Given the importance of APOE lipidation in AD pathophysiology, further studies are needed to better understand the roles of ABCA1 and ABCG1 in RXR-mediated brain responses across cell subtypes and disease stages.

LXR/RXR, PPAR/RXR, and RAR/RXR play roles in the brain metabolic dysfunctions associated with AD [10,20,75]. Thus, bexarotene's metabolic effects reflect a complex network of NR signaling pathways, likely combining synergistic and conflicting responses. Our findings show that bexarotene significantly activates cholesterol and lipid biosynthesis pathways in homeostatic astrocytes, indicating an increase in astrocyte-derived cholesterol metabolism. In a previous study, we demonstrated that LXR/RXR activation by LXL ligand leads to similar changes in mice carrying APP mutation (*Scd1*, *Scd2*, *Lpcat3*, *Mid1lipl*, *Srebf1*), corroborating our results [22]. Cholesterol synthesis and APOE-mediated transport are essential for brain repair [4]. Cholesterol delivered to other brain cells influences neuronal neurotransmitter release, synaptic activity, oligodendrocyte myelination, and OPC proliferation and migration [3]. The upregulated cholesterol synthesis pathway in oligodendrocytes, distinct from that in astrocytes, may be tailored to meet local demands [76]. The regulation of cholesterol synthesis, CREB signaling, and *Apoe/Apod* expression in oligodendrocytes in Bexa may support brain remyelination, especially at advanced stages of neuronal and myelin loss [56,58,77]. Therefore, the activation of lipid metabolism in APP/PS1 astrocytes and oligodendrocytes may be connected to the observed neurorepair following brain RXR activation [10].

In a previous bulk RNA-seq study, we showed that six-month-old APP/PS1 mice treated with bexarotene display upregulated *Apoe*, *Apod*, *Fcrls*, and *C1q* genes, as well as other DAM genes [18]. This corroborates our present findings in microglia, reactive astrocytes, and oligodendrocytes, although other classical DAM genes were not affected and we did not find increased DAM proportions in Bexa. Furthermore, the single-cell transcriptional profiles revealed the modulation of immune-associated gene responses in distinct brain cells. Bexarotene activated immunoreactivity genes in reactive astrocytes and the classical DAM subpopulation while downregulating DAM- and plaque-associated genes in homeostatic populations. In parallel, ECs showed downregulated immune activity. These findings highlight the selective enhancement of immune features in reactive cells. Since increased DAM and immune-cell reactivity are established features of AD, and a loss of DAM function is linked to worsened pathology [46], the drug-induced upregulation of genes like *Apoe*, *Anxa3*, *C1qc*, and *Fcrls* aligns with its therapeutic effect.

Bexarotene-induced *Apoe* upregulation was most prominent in DAM microglia, where APOE is a key feature of DAM states linked to the engulfment of apoptotic bodies and myelin debris [46]. APOE also regulates microglial interaction with Aβ and plays a crucial role in plaque compaction [53,54]. Similarly, chromatin accessibility peaks linked to the apolipoprotein *locus*, including *Apoe*, are significantly upregulated by Bexa in microglia [41]. Furthermore, astrocytes contribute to Aβ degradation in an APOE-dependent manner, and deficits in astroglial Aβ clearance are implicated in AD pathogenesis [43,44]. The putative increase in Bexa-associated APOE signaling suggests activated Aβ processing and downstream cell activation through the APOE/TREM2 axis. Notably, bexarotene enhances immune cell phagocytic activity [18,26]. Additionally, APOE-dependent regulation of cholesterol in lipid rafts links to its immunomodulatory roles. In activated microglia, cholesterol enrichment enhances phagocytosis and the release of neurotrophic factors [52]. Thus, the combination of high *Apoe* and low *Abca1/Abcg1* observed especially in the DAM phenotype may contribute to immune signaling transduction.

Previous studies have shown reduced neuroinflammation following RXR activation in AD models, consistent with our findings. In an APP/PS1 mouse model, bexarotene treatment was shown to activate the brain gene expression of the anti-inflammatory cytokines TGF-β and IL-6 and transcription factor ATF3 while also activating CCL2 gene expression, which is important for microglial accumulation in inflammatory sites and reducing the pro-inflammatory IL-1β [19]. Similarly, the treatment reversed the expression of pro-inflammatory markers and reduced astrogliosis in 5XFAD mouse brains [12]. In our study, we observed an increase in the TGF-β pathway, especially from homeostatic astrocytes towards microglia. Impairment of the TGF-β pathway is a feature of AD-linked neuroinflammation [69], which indicates a beneficial role of bexarotene. PPAR activation antagonizes NF-κB signaling through TGF-β production [37], which may explain bexarotene's effects. These findings highlight RXR activation's dual role in immune responses: enhancing APOE-dependent DAM responses while reducing neuroinflammation.

These immune-related events were accompanied by decreased oxidative stress and injury responses in astrocytes and microglia and increased protein folding and HSP responses in oligodendrocytes and ECs. HSP activation occurs in response to UPR to resolve ER stress, maintain proteostasis, and control cytotoxicity [78]. In APP transgenic mice, chaperones like *Hsp70* and *Hsp90* are downregulated, and their overexpression mitigates AD pathology [79,80]. Furthermore, extracellular HSPs are known to be neuroprotective and anti-inflammatory [81,82]. Therefore, their upregulation here aligns with the beneficial effects of RXR activation, likely linked to bexarotene's neuroprotective regulation of Aβ-induced ER stress [60]. Furthermore, protein folding responses are connected to

PPARγ and LXR signaling and lipogenesis [83], which may link to the effects observed in oligodendrocytes. In ECs, it is also connected to cell growth and vasculogenesis [65,66].

Our findings indicate that bexarotene promotes brain regeneration by activating key developmental pathways. Single-cell RNA-seq analysis revealed that this effect is particularly strong in astroglia but also occurs in oligodendrocyte lineage cells and brain endothelial cells, which we further demonstrated in scATA-seq integrative analyses [41]. Using bulk RNA-seq, we previously showed that bexarotene treatment activates brain development-associated genome events in AD mice, specifically *Notch1*, *Notch2*, and *Dlk1* [27,28]. In the single-cell profiles, we observed the upregulation of SOX, HES, and Id family genes, which are directly or indirectly controlled by the Notch signaling pathway [84], thus suggesting a consequence of Notch signaling modulation. This transcriptional profile is also consistent with our previous observation of bexarotene's ability to promote SOX2+/+ symmetric division in adult NSC, a process critical for regeneration [29]. Furthermore, the treatment activated subcluster-specific cell growth markers, like *AC149090.1*, within astrocytes and oligodendrocytes, which may act so as to link metabolic responses to brain development [39].

The Bexa-upregulated *Sox*, *Hes*, and *Id* regulate adult neurogenesis at multiple levels, usually by blocking the activation of proneural factors and maintaining self-renewal in progenitors [85]. In both an AD transgenic mouse model and human AD patients, decreased *Sox2* levels, which correlate with disease severity, suggest that restoring its expression could be a beneficial therapeutic strategy [86]. In glial differentiation, SOX2 deficiency in mature astrocytes compromises cell maturation and glutamate uptake [87]. Thus, the activation of these features in astroglia could explain the increased astrogenesis observed in vitro following bexarotene treatment [29]. In oligodendrocytes, the upregulation of neurokinins and developmental genes, combined with changes in lipid metabolism and the CREB pathway, aligns with prior observations of remyelination activation in bexarotene-treated AD mice [31]. Additionally, RXRγ and 9-cis-RA are linked to OPC proliferation, differentiation, and myelination [30]. Although we did not achieve sufficient resolution to identify OPC-specific responses to bexarotene, future studies could address this, especially in AD and other demyelination-related conditions.

The upregulation in *Sox*, *Hes*, and *Id* family genes was also observed in capillary/arteriole EC, with associated modulation of genes linked to vasculogenesis and increased VEGF signaling. In AD, ECs exhibit apoptosis and senescence, but these effects can be reversed by EC growth stimuli [88]. Similarly, a human brain vascular atlas of AD revealed downregulated angiogenesis, proliferation, and cell motility in capillary and arterial EC [89]. For instance, GLUT1 levels are reduced in AD brain endothelium, which contributes to neuronal loss and brain inflammation [6,90], so the bexarotene-induced upregulation of its encoding gene *Slc2a1* might be beneficial. However, excessive VEGF signaling and non-productive angiogenesis, often observed in AD, contribute to the vascular imbalance [7]. The concurrent pro- and anti-proliferative signatures we detected may reflect this balance. Therefore, we demonstrate that brain activation of RXR supports developmental pathways and cell growth within ECs, suggesting a role in promoting vascular activation and integrity. However, the significance of this angiogenesis-related effect in AD requires further investigation.

Lastly, these results must be interpreted considering this study's limitations. Our previous studies with chromatin remodeling analysis and whole-brain transcriptional analysis corroborate the results linked to apolipoprotein, immune-associated markers, lipid metabolism, and neurodevelopmental genes [18,19,22,28,41], but we did not validate some of the newly discovered pathways and gene sets. The fold changes we observed are more modest than those reported in these and other bulk RNA-seq studies with similar treat-

ments, likely reflecting the loss of high fold-change DEGs in single-cell platforms compared to bulk [91]. Furthermore, the functional analyses based on GO terms and cell communication pathways are predictions based on gene expression data. Thus, the connection of bexarotene treatment to specific biological processes in these cell types should be further explored in mechanistic experiments using both in vivo and in vitro models, which will help clarify the biological significance of the gene expression changes. Furthermore, the lack of wild-type mice limits the interpretation of disease-specific transcriptional effects of bexarotene, which may be different for specific AD mouse models and disease stages. In this regard, we have previously shown that for some DAM genes, activation by bexarotene occurs selectively in AD mice and is not observed in WT mice [18], whereas chromatin immunoprecipitation data revealed conserved RXR binding at neurodevelopmental loci even in the WT context [28]. Despite these limitations, this study provides the first comprehensive, single-cell atlas of transcriptional responses to NR heterodimer activation in an AD context, revealing a coordinated multicellular program.

4. Materials and Methods

4.1. Animals

APP/PS1 mice were purchased from The Jackson Laboratory (Bar Harbor, ME, USA), featuring the mutations APP K670_M671delinsNL (Swedish) and PSEN1:deltaE9. Cortical amyloid plaques begin to develop at three months of age and increase in size and number as the mice age. For experiments, animals were bred in-house as heterozygotes. Experimental mice were housed in groups of five females or four males per cage. Animals were littermates and maintained on a 12 h light/dark cycle with ad libitum food and water. Both male and female mice were used in the experiments. All animal procedures adhered to the Guide for the Care and Use of Laboratory Animals from the United States Department of Health and Human Services and were approved by the University of Pittsburgh Institutional Animal Care and Use Committee. All experiments were conducted in compliance with the ARRIVE guidelines.

4.2. Mouse Treatment

We randomly assigned eight five-month-old APP/PS1 mice to either the Bexa group (100 mg/kg/day bexarotene) or the Ctrl group (vehicle treatment), ensuring a balanced distribution by age and sex, with two males and two females for each treatment and further analysis. Bexarotene (Alfa Aesar, Ward Hill, MA, USA) was prepared in a vehicle solution of corn oil containing 1% DMSO on the day of treatment. The animals received 10 µL/g of either bexarotene or vehicle solution by oral gavage for ten consecutive days (Table S2) [17,18]. The animals were monitored daily, and loss of $\geq$10% body weight was used as the humane endpoint.

For euthanasia, mice were anesthetized with Avertin (1.25% tribromoethanol, 2.5% 2-methyl-2-butanol, 250 mg/kg IP administration). Blood was collected via cardiac puncture of the right ventricle with EDTA-treated syringes, followed by transcardial perfusion with 20 mL of PBS. One brain hemisphere was dissected and immediately processed for brain dissociation and subsequent single-cell analysis. Relative to blinding, only the lab technician was aware of the group allocation at all stages until data analysis.

4.3. Neural Tissue Dissociation

We immediately processed freshly dissected mouse brain hemispheres, after removing the cerebellum, olfactory bulb, and subcortex, using the Adult Brain Dissociation Kit (Miltenyi Biotec, Macquarie Park, Australia) for mouse and rat, with slight modifications to the manufacturer's protocol. Briefly, neural tissues were dissected into small pieces

in HBSS, and tissue pellets were incubated with enzyme mix P/Z (containing 0.125% 2-mercaptoethanol) for 15 min at 37 °C, with gentle rotation every 2 min. Next, enzyme mix Y/A was added to the samples, and the tissues were then mechanically dissociated by gentle pipetting and incubated for 10 min at 37 °C with gentle rotation every 2 min. Samples were mechanically dissociated and incubated again for another 10 min at 37 °C. The resulting suspensions were filtered through moistened 40 µm cell strainers (Corning, Corning, NY, USA) and washed with HBSS (1:5). We then removed tissue debris using Debris Removal Solution (Miltenyi Biotec), following manufacturer's instructions. Cell pellets were washed once using 0.04% BSA-DPBS buffer and filtered through 40 µm Flowmi cell strainers (Bel-Art, Wayne, NJ, USA) before cell counting under the microscope using Trypan Blue. Cell viability ranged from 85 to 95% (Table S2).

4.4. Single-Cell Transcriptomics

Droplet-based scRNA-seq library generation was prepared using Chromium Next GEM Single Cell 3′ Kit v3.1 and Chip G Single Cell Kit (10x Genomics, Pleasanton, CA, USA) according to the manufacturer's instructions. Immediately after tissue dissociation, Ctrl- and Bexa-derived single-cell suspensions (four samples each) were used for GEM generation and barcoding in Chromium Controller (10x Genomics), with 10,000 cells as targeted recovery for each sample (Table S2). After cleanup, 25–75 ng of barcoded cDNA was amplified for library construction, and Dual Index Kit TT Set A (10x Genomics) was used for sample indexing. Library quality control was checked by Bioanalyzer High Sensitivity DNA kit (Agilent, Santa Clara, CA, USA) (Table S2), and sequencing was performed on Illumina NovaSeq SP PE100 (MedGenome Inc., Bangalore, India), targeting 400 M reads per library.

4.5. Data Preprocessing

Single-cell barcoded reads were demultiplexed and aligned to the mouse reference genome (GRCm38) using Cell Ranger pipeline v7.0 (10x Genomics). The matrices of unique molecular identifiers (UMIs) generated by Cell Ranger were read into R v4.2.0 and analyzed using Seurat v4.2.1 [34], as previously described [48]. Before processing, approximately 6000 cells were sampled per library. The initial cell quality control step filtered only the cells with (i) unique feature counts >200 and <5000, (ii) total counts <50,000, and (iii) percentage of mitochondrial gene counts <10, which resulted in a matrix with total of 23,745 genes across 37,634 cells. SCTransform [33] was employed for feature normalization and scaling as well as variable feature analysis. We performed principal component (PC) analysis using variable features (RunPCA), followed by unsupervised clustering analysis (FindNeighbors using top 10 PCs, and FindClusters with 0.25 resolution). Uniform Manifold Approximation and Projection (UMAP) analysis was employed for dimensional reduction and data visualization (RunUMAP using top 10 PCs).

4.6. Differential Expression Analysis

Clusters' differential expression was performed using MAST v1.22.0 [92] within Seurat FindMarkers, then manually annotated based on the expression levels of cell-type-specific gene sets (Table S2). Marker genes for cell types were selected based on previous publications [42,47,55]. Next, selected cell types were further analyzed as subsets and similarly pre-processed. The mean expression of cell-type-specific gene sets was added to the matrices using AddModuleScore, and an additional cell filtering step removed subclusters or cells expressing non-selective gene sets. The top marker genes for each subpopulation were selected based on log2 fold change >0.5 and ranked by fold change. Choroid-plexus epithelial cell gene *Ttr* and hemoglobin genes (*Hb*-) were disregarded in further analysis. Cell-type-specific differential analysis between Bexa and Ctrl groups was performed using

MAST testing within Seurat. Differentially expressed genes (DEG) were defined according to adj. p-value < 0.05 and either pct.1 (fraction of expressing cells in Bexa) or pct.2 (fraction of expressing cells in Ctrl) > 0.2.

4.7. Gene Ontology and Pathway Analysis

Functional annotation of gene ontologies was performed using DAVID v6.8 web-tool [93], Cluster Profiler v4.6.2 gene set enrichment analysis with gseGO function [94], and Pathview for construction of pathway maps [95]. To construct the graphs, we used p-value and DEG counts.

4.8. Cell Communication Inference

We used CellChat v2 [67] to infer, analyze, and visualize cell–cell communication networks. The analysis input was a merged, preprocessed gene expression matrix from the subclusters Astro–Homeostatic, Astro–Reactive, Micro–Homeostatic, Micro–DAM, oligodendrocytes, and Endothelial–Capillary/Arteriole for each condition. We preprocessed and analyzed individual Ctrl and Bexa matrices with CellChat to separately compute communication probabilities among cells and create independent cellular communication networks using computeCommunProb (with "trimean" as the method). We selected secreted signaling, ECM–receptor, and cell–cell contact pathways from CellChatDB, a manually curated ligand-receptor interaction database, for analysis.

Next, the networks were merged to compare Bexa vs. Ctrl. The differential number of interactions and the differential interaction strength were inferred using the functions compareInteractions and netVisual_diffInteractions. Interaction strength represents the computed communication probability, derived from two centrality measures: outdegree and indegree with weights. We assessed overall and cell pair-specific changes in signaling pathways by analyzing information flows, which are the sum of communication probabilities among all cell group pairs in the inferred network. We used the rankNet function, considering weights as measure. Finally, we evaluated changes in incoming and outgoing signaling pathways for specific cell populations using net analysis functions (netAnalysis_signalingRole_scatter and netAnalysis_signalingChanges_scatter).

4.9. Statistical Analysis

Sample sizes are indicated in the legends and correspond to biological replicates. Power analysis was performed to estimate the number of animals (two groups, t test, G*Power v3.1, Dusseldorf, Germany) with individual estimated experimental effect size, alpha = 0.05, and 95% power. Statistical analyses referring to differential expression results were performed in R v4.2.0 using MAST v1.22.0 testing within Seurat, and significance was determined as Bonferroni-corrected p-value < 0.05 (adj.p-value). Cluster distribution among libraries was analyzed on GraphPad Prism v8.0.2 (Boston, MA, USA) using two-way ANOVA, and significance for the effect of treatment was determined as p-value < 0.05. DAVID v6.8 GO analysis used Fisher's exact test, considering uncorrected p-value < 0.05. Cell communication inference with CellChat v2 used paired Wilcoxon test considering permutation-based p-value < 0.05, with explicit thresholds to control for false-positive interaction predictions (thresh = 1). Unless otherwise indicated in figure legends, results are reported as means with error bars as standard error (SEM).

5. Conclusions

In conclusion, our study delineates the cellular origins of known RXR-directed effects while uncovering novel, cell-type-specific responses. We demonstrate that the well-documented *Apoe* upregulation is orchestrated across multiple brain cells, including microglia, reactive astrocytes, and oligodendrocytes. Similarly, we point to homeostatic

astrocytes and oligodendrocytes as key mediators of bexarotene's developmental and metabolic effects and delineate subpopulation-specific immune responses to RXR activation. Besides that, this study reveals novel dimensions of the drug's activity, such as endothelial-specific mechanisms and protein refolding transcriptional responses. Collectively, the results highlight RXR and APOE biology as tools for developing multi-faceted therapies that modulate diverse biological processes—including cholesterol biosynthesis, lipid metabolism, neurodevelopment, cell growth, heat shock response, and immune reactivity—within specific brain cells while opening new avenues to explore RXR-controlled networks in context-specific processes such as angiogenesis and protein homeostasis.

Supplementary Materials: The following supporting information can be downloaded at https://www.mdpi.com/article/10.3390/ijms27052435/s1.

Author Contributions: Conceptualization, R.K., I.L., N.F.F. and C.S.-G.; Methodology, C.S.-G., Y.L. and N.F.F.; Investigation, C.S.-G., Y.L. and N.F.F.; Formal Analysis, C.S.-G.; Visualization, C.S.-G.; Writing—Original Draft, C.S.-G.; Writing—Review and Editing, C.S.-G., R.K., I.L. and D.P.G.; Supervision, R.K., I.L. and D.P.G.; Project Administration, R.K. and I.L.; Resources, R.K. and I.L.; Funding Acquisition R.K. and I.L. All authors have read and agreed to the published version of the manuscript.

Funding: This work was funded by the National Institutes of Health, USA (R01 AG066198; R01 AG077636; R01 AG075992; R01 AG057565 and R01 AG075069). Carolina Saibro-Girardi was supported by scholarships from the Coordination for the Improvement of Higher Education Personnel (CAPES) and the National Council for Scientific and Technological Development (CNPq), Brazil.

Institutional Review Board Statement: All animal procedures were performed according to the Guide for the Care and Use of Laboratory Animals from the United States Department of Health and Human Services and were approved by the University of Pittsburgh Institutional Animal Care and Use Committee (Approval Code: PHS Assurance Number D16-00118; Approval Date: 16 March 2022).

Informed Consent Statement: Not applicable.

Data Availability Statement: Raw data single-cell RNA-seq are publicly available at GEO (https://www.ncbi.nlm.nih.gov/geo/ (accessed on 20 February 2026), GEO accession: GSE283905). This paper does not report the original code. Any additional information required to reanalyze the data reported in this paper is available from the corresponding author upon request.

Acknowledgments: The authors thank Mikayla Ranae McGuire and Mary Ann Ostach for their technical support.

Conflicts of Interest: The authors declare no conflicts of interest.

References

1. Knopman, D.S.; Amieva, H.; Petersen, R.C.; Chetelat, G.; Holtzman, D.M.; Hyman, B.T.; Nixon, R.A.; Jones, D.T. Alzheimer disease. *Nat. Rev. Dis. Primers* **2021**, *7*, 33. [CrossRef]
2. Wolfe, C.M.; Fitz, N.F.; Nam, K.N.; Lefterov, I.; Koldamova, R. The Role of APOE and TREM2 in Alzheimer's Disease-Current Understanding and Perspectives. *Int. J. Mol. Sci.* **2018**, *20*, 81. [CrossRef] [PubMed]
3. Li, D.; Zhang, J.; Liu, Q. Brain cell type-specific cholesterol metabolism and implications for learning and memory. *Trends Neurosci.* **2022**, *45*, 401–414. [CrossRef]
4. Amany, M.; Kevan, S.; de Chaves, E.P. The Mevalonate Pathway in Alzheimer's Disease—Cholesterol and Non-Sterol Isoprenoids. In *Alzheimer's Disease*; Inga, Z., Ed.; IntechOpen: Rijeka, Croatia, 2015; Chapter 7.
5. Ho, Y.S.; Yang, X.; Lau, J.C.; Hung, C.H.; Wuwongse, S.; Zhang, Q.; Wang, J.; Baum, L.; So, K.F.; Chang, R.C. Endoplasmic reticulum stress induces tau pathology and forms a vicious cycle: Implication in Alzheimer's disease pathogenesis. *J. Alzheimers Dis.* **2012**, *28*, 839–854. [CrossRef]
6. Sweeney, M.D.; Sagare, A.P.; Zlokovic, B.V. Blood-brain barrier breakdown in Alzheimer disease and other neurodegenerative disorders. *Nat. Rev. Neurol.* **2018**, *14*, 133–150. [CrossRef]
7. Love, S.; Miners, J.S. Cerebrovascular disease in ageing and Alzheimer's disease. *Acta Neuropathol.* **2016**, *131*, 645–658. [CrossRef]

8. Lee, S.; Viqar, F.; Zimmerman, M.E.; Narkhede, A.; Tosto, G.; Benzinger, T.L.; Marcus, D.S.; Fagan, A.M.; Goate, A.; Fox, N.C.; et al. White matter hyperintensities are a core feature of Alzheimer's disease: Evidence from the dominantly inherited Alzheimer network. *Ann. Neurol.* **2016**, *79*, 929–939. [CrossRef]
9. Salta, E.; Lazarov, O.; Fitzsimons, C.P.; Tanzi, R.; Lucassen, P.J.; Choi, S.H. Adult hippocampal neurogenesis in Alzheimer's disease: A roadmap to clinical relevance. *Cell Stem Cell* **2023**, *30*, 120–136. [CrossRef] [PubMed]
10. Fitz, N.F.; Nam, K.N.; Koldamova, R.; Lefterov, I. Therapeutic targeting of nuclear receptors, liver X and retinoid X receptors, for Alzheimer's disease. *Br. J. Pharmacol.* **2019**, *176*, 3599–3610. [CrossRef]
11. Evans, R.M.; Mangelsdorf, D.J. Nuclear Receptors, RXR, and the Big Bang. *Cell* **2014**, *157*, 255–266. [CrossRef]
12. Mariani, M.M.; Malm, T.; Lamb, R.; Jay, T.R.; Neilson, L.; Casali, B.; Medarametla, L.; Landreth, G.E. Neuronally-directed effects of RXR activation in a mouse model of Alzheimer's disease. *Sci. Rep.* **2017**, *7*, 42270. [CrossRef] [PubMed]
13. Muñoz-Cabrera, J.M.; Sandoval-Hernández, A.G.; Niño, A.; Báez, T.; Bustos-Rangel, A.; Cardona-Gómez, G.P.; Múnera, A.; Arboleda, G. Bexarotene therapy ameliorates behavioral deficits and induces functional and molecular changes in very-old Triple Transgenic Mice model of Alzheimer's disease. *PLoS ONE* **2019**, *14*, e0223578. [CrossRef]
14. Cramer, P.E.; Cirrito, J.R.; Wesson, D.W.; Lee, C.Y.; Karlo, J.C.; Zinn, A.E.; Casali, B.T.; Restivo, J.L.; Goebel, W.D.; James, M.J.; et al. ApoE-directed therapeutics rapidly clear β-amyloid and reverse deficits in AD mouse models. *Science* **2012**, *335*, 1503–1506. [CrossRef]
15. Veeraraghavalu, K.; Zhang, C.; Miller, S.; Hefendehl, J.K.; Rajapaksha, T.W.; Ulrich, J.; Jucker, M.; Holtzman, D.M.; Tanzi, R.E.; Vassar, R.; et al. Comment on "ApoE-directed therapeutics rapidly clear β-amyloid and reverse deficits in AD mouse models". *Science* **2013**, *340*, 924. [CrossRef]
16. Boehm-Cagan, A.; Michaelson, D.M. Reversal of apoE4-driven brain pathology and behavioral deficits by bexarotene. *J. Neurosci.* **2014**, *34*, 7293–7301. [CrossRef]
17. Fitz, N.F.; Cronican, A.A.; Lefterov, I.; Koldamova, R. Comment on "ApoE-directed therapeutics rapidly clear β-amyloid and reverse deficits in AD mouse models". *Science* **2013**, *340*, 924. [CrossRef]
18. Lefterov, I.; Schug, J.; Mounier, A.; Nam, K.N.; Fitz, N.F.; Koldamova, R. RNA-sequencing reveals transcriptional up-regulation of Trem2 in response to bexarotene treatment. *Neurobiol. Dis.* **2015**, *82*, 132–140. [CrossRef] [PubMed]
19. Corona, A.W.; Kodoma, N.; Casali, B.T.; Landreth, G.E. ABCA1 is Necessary for Bexarotene-Mediated Clearance of Soluble Amyloid Beta from the Hippocampus of APP/PS1 Mice. *J. Neuroimmune Pharmacol.* **2016**, *11*, 61–72. [CrossRef]
20. Zhao, J.; Fu, Y.; Liu, C.C.; Shinohara, M.; Nielsen, H.M.; Dong, Q.; Kanekiyo, T.; Bu, G. Retinoic acid isomers facilitate apolipoprotein E production and lipidation in astrocytes through the retinoid X receptor/retinoic acid receptor pathway. *J. Biol. Chem.* **2014**, *289*, 11282–11292. [CrossRef] [PubMed]
21. Dickey, A.S.; Sanchez, D.N.; Arreola, M.; Sampat, K.R.; Fan, W.; Arbez, N.; Akimov, S.; Van Kanegan, M.J.; Ohnishi, K.; Gilmore-Hall, S.K.; et al. PPARδ activation by bexarotene promotes neuroprotection by restoring bioenergetic and quality control homeostasis. *Sci. Transl. Med.* **2017**, *9*, eaal2332. [CrossRef]
22. Carter, A.Y.; Letronne, F.; Fitz, N.F.; Mounier, A.; Wolfe, C.M.; Nam, K.N.; Reeves, V.L.; Kamboh, H.; Lefterov, I.; Koldamova, R. Liver X receptor agonist treatment significantly affects phenotype and transcriptome of APOE3 and APOE4 Abca1 haplo-deficient mice. *PLoS ONE* **2017**, *12*, e0172161. [CrossRef] [PubMed]
23. Riancho, J.; Ruiz-Soto, M.; Berciano, M.T.; Berciano, J.; Lafarga, M. Neuroprotective Effect of Bexarotene in the SOD1(G93A) Mouse Model of Amyotrophic Lateral Sclerosis. *Front. Cell Neurosci.* **2015**, *9*, 250. [CrossRef]
24. Zuo, Y.; Huang, L.; Enkhjargal, B.; Xu, W.; Umut, O.; Travis, Z.D.; Zhang, G.; Tang, J.; Liu, F.; Zhang, J.H. Activation of retinoid X receptor by bexarotene attenuates neuroinflammation via PPARγ/SIRT6/FoxO3a pathway after subarachnoid hemorrhage in rats. *J. NeuroInflamm.* **2019**, *16*, 47. [CrossRef] [PubMed]
25. He, J.; Liu, H.; Zhong, J.; Guo, Z.; Wu, J.; Zhang, H.; Huang, Z.; Jiang, L.; Li, H.; Zhang, Z.; et al. Bexarotene protects against neurotoxicity partially through a PPARγ-dependent mechanism in mice following traumatic brain injury. *Neurobiol. Dis.* **2018**, *117*, 114–124. [CrossRef]
26. Chang, C.F.; Massey, J.; Osherov, A.; Angenendt da Costa, L.H.; Sansing, L.H. Bexarotene Enhances Macrophage Erythrophagocytosis and Hematoma Clearance in Experimental Intracerebral Hemorrhage. *Stroke* **2020**, *51*, 612–618. [CrossRef]
27. Nam, K.N.; Mounier, A.; Fitz, N.F.; Wolfe, C.; Schug, J.; Lefterov, I.; Koldamova, R. RXR controlled regulatory networks identified in mouse brain counteract deleterious effects of Aβ oligomers. *Sci. Rep.* **2016**, *6*, 24048. [CrossRef]
28. Mounier, A.; Georgiev, D.; Nam, K.N.; Fitz, N.F.; Castranio, E.L.; Wolfe, C.M.; Cronican, A.A.; Schug, J.; Lefterov, I.; Koldamova, R. Bexarotene-Activated Retinoid X Receptors Regulate Neuronal Differentiation and Dendritic Complexity. *J. Neurosci.* **2015**, *35*, 11862–11876. [CrossRef]
29. Saibro-Girardi, C.; Scheibel, I.M.; Santos, L.; Bittencourt, R.R.; Fröhlich, N.T.; Dos Reis Possa, L.; Moreira, J.C.F.; Gelain, D.P. Bexarotene drives the self-renewing proliferation of adult neural stem cells, promotes neuron-glial fate shift, and regulates late neuronal differentiation. *J. Neurochem.* **2024**, *168*, 1527–1545. [CrossRef]

30. Huang, J.K.; Jarjour, A.A.; Nait Oumesmar, B.; Kerninon, C.; Williams, A.; Krezel, W.; Kagechika, H.; Bauer, J.; Zhao, C.; Baron-Van Evercooren, A.; et al. Retinoid X receptor gamma signaling accelerates CNS remyelination. *Nat. Neurosci.* **2011**, *14*, 45–53. [CrossRef]
31. Santos-Gil, D.F.; Arboleda, G.; Sandoval-Hernández, A.G. Retinoid X receptor activation promotes re-myelination in a very old triple transgenic mouse model of Alzheimer's disease. *Neurosci. Lett.* **2021**, *750*, 135764. [CrossRef] [PubMed]
32. Radde, R.; Bolmont, T.; Kaeser, S.A.; Coomaraswamy, J.; Lindau, D.; Stoltze, L.; Calhoun, M.E.; Jäggi, F.; Wolburg, H.; Gengler, S.; et al. Abeta42-driven cerebral amyloidosis in transgenic mice reveals early and robust pathology. *EMBO Rep.* **2006**, *7*, 940–946. [CrossRef]
33. Hafemeister, C.; Satija, R. Normalization and variance stabilization of single-cell RNA-seq data using regularized negative binomial regression. *Genome Biol.* **2019**, *20*, 296. [CrossRef]
34. Hao, Y.; Hao, S.; Andersen-Nissen, E.; Mauck, W.M.; Zheng, S.; Butler, A.; Lee, M.J.; Wilk, A.J.; Darby, C.; Zager, M.; et al. Integrated analysis of multimodal single-cell data. *Cell* **2021**, *184*, 3573–3587.E29. [CrossRef] [PubMed]
35. Habib, N.; McCabe, C.; Medina, S.; Varshavsky, M.; Kitsberg, D.; Dvir-Szternfeld, R.; Green, G.; Dionne, D.; Nguyen, L.; Marshall, J.L.; et al. Disease-associated astrocytes in Alzheimer's disease and aging. *Nat. Neurosci.* **2020**, *23*, 701–706. [CrossRef]
36. Escartin, C.; Galea, E.; Lakatos, A.; O'Callaghan, J.P.; Petzold, G.C.; Serrano-Pozo, A.; Steinhäuser, C.; Volterra, A.; Carmignoto, G.; Agarwal, A.; et al. Reactive astrocyte nomenclature, definitions, and future directions. *Nat. Neurosci.* **2021**, *24*, 312–325. [CrossRef]
37. Xu, P.; Zhai, Y.; Wang, J. The Role of PPAR and Its Cross-Talk with CAR and LXR in Obesity and Atherosclerosis. *Int. J. Mol. Sci.* **2018**, *19*, 1260. [CrossRef]
38. Lalloyer, F.; Pedersen, T.A.; Gross, B.; Lestavel, S.; Yous, S.; Vallez, E.; Gustafsson, J.A.; Mandrup, S.; Fiévet, C.; Staels, B.; et al. Rexinoid bexarotene modulates triglyceride but not cholesterol metabolism via gene-specific permissivity of the RXR/LXR heterodimer in the liver. *Arter. Thromb. Vasc. Biol.* **2009**, *29*, 1488–1495. [CrossRef]
39. Buckley, M.T.; Sun, E.D.; George, B.M.; Liu, L.; Schaum, N.; Xu, L.; Reyes, J.M.; Goodell, M.A.; Weissman, I.L.; Wyss-Coray, T.; et al. Cell-type-specific aging clocks to quantify aging and rejuvenation in neurogenic regions of the brain. *Nat. Aging* **2023**, *3*, 121–137. [CrossRef] [PubMed]
40. Mizrak, D.; Levitin, H.M.; Delgado, A.C.; Crotet, V.; Yuan, J.; Chaker, Z.; Silva-Vargas, V.; Sims, P.A.; Doetsch, F. Single-Cell Analysis of Regional Differences in Adult V-SVZ Neural Stem Cell Lineages. *Cell Rep.* **2019**, *26*, 394–406.E5. [CrossRef] [PubMed]
41. Lu, Y.; Wang, X.; Saibro-Girardi, C.; Fitz, N.F.; Koldamova, R.; Lefterov, I. RXR-Mediated Remodeling of Transcriptional and Chromatin Landscapes in APP Mouse Brain: Insights from Integrated Single-Cell RNA and ATAC Profiling. *Cells* **2025**, *14*, 1970. [CrossRef]
42. Sadick, J.S.; O'Dea, M.R.; Hasel, P.; Dykstra, T.; Faustin, A.; Liddelow, S.A. Astrocytes and oligodendrocytes undergo subtype-specific transcriptional changes in Alzheimer's disease. *Neuron* **2022**, *110*, 1788–1805.E10. [CrossRef]
43. Wyss-Coray, T.; Loike, J.D.; Brionne, T.C.; Lu, E.; Anankov, R.; Yan, F.; Silverstein, S.C.; Husemann, J. Adult mouse astrocytes degrade amyloid-beta in vitro and in situ. *Nat. Med.* **2003**, *9*, 453–457. [CrossRef]
44. Koistinaho, M.; Lin, S.; Wu, X.; Esterman, M.; Koger, D.; Hanson, J.; Higgs, R.; Liu, F.; Malkani, S.; Bales, K.R.; et al. Apolipoprotein E promotes astrocyte colocalization and degradation of deposited amyloid-beta peptides. *Nat. Med.* **2004**, *10*, 719–726. [CrossRef]
45. Michetti, F.; D'Ambrosi, N.; Toesca, A.; Puglisi, M.A.; Serrano, A.; Marchese, E.; Corvino, V.; Geloso, M.C. The S100B story: From biomarker to active factor in neural injury. *J. Neurochem.* **2019**, *148*, 168–187. [CrossRef] [PubMed]
46. Deczkowska, A.; Keren-Shaul, H.; Weiner, A.; Colonna, M.; Schwartz, M.; Amit, I. Disease-Associated Microglia: A Universal Immune Sensor of Neurodegeneration. *Cell* **2018**, *173*, 1073–1081. [CrossRef] [PubMed]
47. Keren-Shaul, H.; Spinrad, A.; Weiner, A.; Matcovitch-Natan, O.; Dvir-Szternfeld, R.; Ulland, T.K.; David, E.; Baruch, K.; Lara-Astaiso, D.; Toth, B.; et al. A Unique Microglia Type Associated with Restricting Development of Alzheimer's Disease. *Cell* **2017**, *169*, 1276–1290.E17. [CrossRef] [PubMed]
48. Lu, Y.; Saibro-Girardi, C.; Fitz, N.F.; McGuire, M.R.; Ostach, M.A.; Mamun-Or-Rashid, A.N.M.; Lefterov, I.; Koldamova, R. Multi-transcriptomics reveals brain cellular responses to peripheral infection in Alzheimer's disease model mice. *Cell Rep.* **2023**, *42*, 112785. [CrossRef]
49. Zhang, Z.; Li, Z.; Ma, Z.; Deng, M.; Xing, M.; Wu, J.; Jiang, S.; Wang, Q.; Guo, Q.; Zou, W. Annexin A3 as a Marker Protein for Microglia in the Central Nervous System of Rats. *Neural Plast.* **2021**, *2021*, 5575090. [CrossRef]
50. Gan, Y.L.; Lin, W.J.; Fang, Y.C.; Tang, C.Y.; Lee, Y.H.; Jeng, C.J. FKBP51 is involved in LPS-induced microglial activation via NF-κB signaling to mediate neuroinflammation. *Life Sci.* **2024**, *351*, 122867. [CrossRef]
51. Luo, R.; Su, L.Y.; Li, G.; Yang, J.; Liu, Q.; Yang, L.X.; Zhang, D.F.; Zhou, H.; Xu, M.; Fan, Y.; et al. Activation of PPARA-mediated autophagy reduces Alzheimer disease-like pathology and cognitive decline in a murine model. *Autophagy* **2020**, *16*, 52–69. [CrossRef]
52. de Dios, C.; Abadin, X.; Roca-Agujetas, V.; Jimenez-Martinez, M.; Morales, A.; Trullas, R.; Mari, M.; Colell, A. Inflammasome activation under high cholesterol load triggers a protective microglial phenotype while promoting neuronal pyroptosis. *Transl. Neurodegener.* **2023**, *12*, 10. [CrossRef]

53. Ulrich, J.D.; Ulland, T.K.; Mahan, T.E.; Nyström, S.; Nilsson, K.P.; Song, W.M.; Zhou, Y.; Reinartz, M.; Choi, S.; Jiang, H.; et al. ApoE facilitates the microglial response to amyloid plaque pathology. *J. Exp. Med.* **2018**, *215*, 1047–1058. [CrossRef] [PubMed]
54. Henningfield, C.M.; Arreola, M.A.; Soni, N.; Spangenberg, E.E.; Green, K.N. Microglia-specific ApoE knock-out does not alter Alzheimer's disease plaque pathogenesis or gene expression. *Glia* **2022**, *70*, 287–302. [CrossRef] [PubMed]
55. Zeisel, A.; Hochgerner, H.; Lönnerberg, P.; Johnsson, A.; Memic, F.; van der Zwan, J.; Häring, M.; Braun, E.; Borm, L.E.; La Manno, G.; et al. Molecular Architecture of the Mouse Nervous System. *Cell* **2018**, *174*, 999–1014.E22. [CrossRef]
56. Blanchard, J.W.; Akay, L.A.; Davila-Velderrain, J.; von Maydell, D.; Mathys, H.; Davidson, S.M.; Effenberger, A.; Chen, C.Y.; Maner-Smith, K.; Hajjar, I.; et al. APOE4 impairs myelination via cholesterol dysregulation in oligodendrocytes. *Nature* **2022**, *611*, 769–779, Correction in *Nature* **2024**, *636*, E9. https://doi.org/10.1038/s41586-024-08434-5. [CrossRef]
57. Sanchez, D.; Ganfornina, M.D. The Lipocalin Apolipoprotein D Functional Portrait: A Systematic Review. *Front. Physiol.* **2021**, *12*, 738991. [CrossRef]
58. García-Mateo, N.; Pascua-Maestro, R.; Pérez-Castellanos, A.; Lillo, C.; Sanchez, D.; Ganfornina, M.D. Myelin extracellular leaflet compaction requires apolipoprotein D membrane management to optimize lysosomal-dependent recycling and glycocalyx removal. *Glia* **2018**, *66*, 670–687. [CrossRef]
59. Narine, M.; Colognato, H. Current Insights Into Oligodendrocyte Metabolism and Its Power to Sculpt the Myelin Landscape. *Front. Cell Neurosci.* **2022**, *16*, 892968. [CrossRef]
60. Dheer, Y.; Chitranshi, N.; Gupta, V.; Abbasi, M.; Mirzaei, M.; You, Y.; Chung, R.; Graham, S.L. Bexarotene Modulates Retinoid-X-Receptor Expression and Is Protective Against Neurotoxic Endoplasmic Reticulum Stress Response and Apoptotic Pathway Activation. *Mol. Neurobiol.* **2018**, *55*, 9043–9056. [CrossRef] [PubMed]
61. Shiga, H.; Asou, H.; Ito, E. Advancement of differentiation of oligodendrocyte progenitor cells by a cascade including protein kinase A and cyclic AMP-response element binding protein. *Neurosci. Res.* **2005**, *53*, 436–441. [CrossRef]
62. Mojzisch, A.; Brehm, M.A. The Manifold Cellular Functions of von Willebrand Factor. *Cells* **2021**, *10*, 2351. [CrossRef]
63. Sawada, J.; Urakami, T.; Li, F.; Urakami, A.; Zhu, W.; Fukuda, M.; Li, D.Y.; Ruoslahti, E.; Komatsu, M. Small GTPase R-Ras regulates integrity and functionality of tumor blood vessels. *Cancer Cell* **2012**, *22*, 235–249. [CrossRef]
64. Ichikawa-Shindo, Y.; Sakurai, T.; Kamiyoshi, A.; Kawate, H.; Iinuma, N.; Yoshizawa, T.; Koyama, T.; Fukuchi, J.; Iimuro, S.; Moriyama, N.; et al. The GPCR modulator protein RAMP2 is essential for angiogenesis and vascular integrity. *J. Clin. Investig.* **2008**, *118*, 29–39. [CrossRef]
65. Lee, Y.J.; Lee, H.J.; Choi, S.H.; Jin, Y.B.; An, H.J.; Kang, J.H.; Yoon, S.S.; Lee, Y.S. Soluble HSPB1 regulates VEGF-mediated angiogenesis through their direct interaction. *Angiogenesis* **2012**, *15*, 229–242. [CrossRef] [PubMed]
66. Meng, J.; Liu, Y.; Han, J.; Tan, Q.; Chen, S.; Qiao, K.; Zhou, H.; Sun, T.; Yang, C. Hsp90β promoted endothelial cell-dependent tumor angiogenesis in hepatocellular carcinoma. *Mol. Cancer* **2017**, *16*, 72. [CrossRef]
67. Jin, S.; Guerrero-Juarez, C.F.; Zhang, L.; Chang, I.; Ramos, R.; Kuan, C.H.; Myung, P.; Plikus, M.V.; Nie, Q. Inference and analysis of cell-cell communication using CellChat. *Nat. Commun.* **2021**, *12*, 1088. [CrossRef]
68. González-Castillo, C.; Ortuño-Sahagún, D.; Guzmán-Brambila, C.; Pallàs, M.; Rojas-Mayorquín, A.E. Pleiotrophin as a central nervous system neuromodulator, evidences from the hippocampus. *Front. Cell Neurosci.* **2014**, *8*, 443. [CrossRef]
69. Vidovic, N.; Spittau, B. Microglial Transforming Growth Factor-β Signaling in Alzheimer's Disease. *Int. J. Mol. Sci.* **2024**, *25*, 3090. [CrossRef]
70. Skerrett, R.; Pellegrino, M.P.; Casali, B.T.; Taraboanta, L.; Landreth, G.E. Combined Liver X Receptor/Peroxisome Proliferator-activated Receptor γ Agonist Treatment Reduces Amyloid β Levels and Improves Behavior in Amyloid Precursor Protein/Presenilin 1 Mice. *J. Biol. Chem.* **2015**, *290*, 21591–21602. [CrossRef]
71. Cummings, J.L.; Zhong, K.; Kinney, J.W.; Heaney, C.; Moll-Tudla, J.; Joshi, A.; Pontecorvo, M.; Devous, M.; Tang, A.; Bena, J. Double-blind, placebo-controlled, proof-of-concept trial of bexarotene Xin moderate Alzheimer's disease. *Alzheimers Res. Ther.* **2016**, *8*, 4. [CrossRef] [PubMed]
72. Velma, G.R.; Laham, M.S.; Lewandowski, C.; Valencia-Olvera, A.C.; Balu, D.; Moore, A.; Ackerman-Berrier, M.; Rychetsky, P.; Penton, C.; Musku, S.R.; et al. Nonlipogenic ABCA1 Inducers (NLAI) for Alzheimer's Disease Validated in a Mouse Model Expressing Human. *J. Med. Chem.* **2024**, *67*, 15061–15079. [CrossRef] [PubMed]
73. Stanek, J.; Swearingen, B.; Strittmatter, W.; Chamberlain, S.; Gabriel, H.; Coutlee, C.; Lineberry, C.; Didsbury, J. Phase 2 PIONEER Trial of Oral T3D-959 for the Treatment of Patients Diagnosed with Mild-to-Moderate Alzheimer's Disease: New Results in a Modified Intent-to-Treat Population. *Alzheimers Dement.* **2024**, *20*, e095625. [CrossRef]
74. Tai, L.M.; Koster, K.P.; Luo, J.; Lee, S.H.; Wang, Y.T.; Collins, N.C.; Ben Aissa, M.; Thatcher, G.R.J.; LaDu, M.J. Amyloid-β pathology and APOE genotype modulate retinoid X receptor agonist activity in vivo. *J. Biol. Chem.* **2014**, *289*, 30538–30555. [CrossRef]
75. Lu, Y.; Fujioka, H.; Wang, W.; Zhu, X. Bezafibrate confers neuroprotection in the 5xFAD mouse model of Alzheimer's disease. *Biochim. Biophys. Acta Mol. Basis Dis.* **2023**, *1869*, 166841. [CrossRef]
76. Barnes-Vélez, J.A.; Aksoy Yasar, F.B.; Hu, J. Myelin lipid metabolism and its role in myelination and myelin maintenance. *Innovation* **2023**, *4*, 100360. [CrossRef] [PubMed]

77. Mathews, E.S.; Appel, B. Cholesterol Biosynthesis Supports Myelin Gene Expression and Axon Ensheathment through Modulation of P13K/Akt/mTor Signaling. *J. Neurosci.* **2016**, *36*, 7628–7639. [CrossRef]
78. Liu, Y.; Chang, A. Heat shock response relieves ER stress. *EMBO J.* **2008**, *27*, 1049–1059. [CrossRef]
79. Hoshino, T.; Murao, N.; Namba, T.; Takehara, M.; Adachi, H.; Katsuno, M.; Sobue, G.; Matsushima, T.; Suzuki, T.; Mizushima, T. Suppression of Alzheimer's disease-related phenotypes by expression of heat shock protein 70 in mice. *J. Neurosci.* **2011**, *31*, 5225–5234. [CrossRef]
80. Wang, B.; Liu, S.; Hao, K.; Wang, Y.; Li, Z.; Lou, Y.; Chang, Y.; Qi, W. HDAC6 modulates the cognitive behavioral function and hippocampal tissue pathological changes of APP/PS1 transgenic mice through HSP90-HSF1 pathway. *Exp. Brain Res.* **2024**, *242*, 1983–1998. [CrossRef]
81. Bobkova, N.V.; Garbuz, D.G.; Nesterova, I.; Medvinskaya, N.; Samokhin, A.; Alexandrova, I.; Yashin, V.; Karpov, V.; Kukharsky, M.S.; Ninkina, N.N.; et al. Therapeutic effect of exogenous hsp70 in mouse models of Alzheimer's disease. *J. Alzheimers Dis.* **2014**, *38*, 425–435. [CrossRef]
82. Tiefensee Ribeiro, C.; Peixoto, D.O.; Santos, L.; Saibro-Girardi, C.; Brum, P.O.; Carazza-Kessler, F.G.; Somensi, N.; Behrens, L.M.P.; Bittencourt, R.R.; Soares, L.S.; et al. Intranasal HSP70 administration protects against dopaminergic denervation and modulates neuroinflammatory response in the 6-OHDA rat model. *Brain Behav. Immun. Health* **2021**, *14*, 100253. [CrossRef]
83. Wheeler, M.C.; Gekakis, N. Hsp90 modulates PPARγ activity in a mouse model of nonalcoholic fatty liver disease. *J. Lipid Res.* **2014**, *55*, 1702–1710. [CrossRef]
84. Lampada, A.; Taylor, V. Notch signaling as a master regulator of adult neurogenesis. *Front. Neurosci.* **2023**, *17*, 1179011. [CrossRef]
85. Boareto, M.; Iber, D.; Taylor, V. Differential interactions between Notch and ID factors control neurogenesis by modulating Hes factor autoregulation. *Development* **2017**, *144*, 3465–3474. [CrossRef] [PubMed]
86. Crews, L.; Adame, A.; Patrick, C.; Delaney, A.; Pham, E.; Rockenstein, E.; Hansen, L.; Masliah, E. Increased BMP6 levels in the brains of Alzheimer's disease patients and APP transgenic mice are accompanied by impaired neurogenesis. *J. Neurosci.* **2010**, *30*, 12252–12262. [CrossRef] [PubMed]
87. Wang, Y.; Zhang, S.; Lan, Z.; Doan, V.; Kim, B.; Liu, S.; Zhu, M.; Hull, V.L.; Rihani, S.; Zhang, C.L.; et al. SOX2 is essential for astrocyte maturation and its deletion leads to hyperactive behavior in mice. *Cell Rep.* **2022**, *41*, 111842. [CrossRef] [PubMed]
88. Georgieva, I.; Tchekalarova, J.; Iliev, D.; Tzoneva, R. Endothelial Senescence and Its Impact on Angiogenesis in Alzheimer's Disease. *Int. J. Mol. Sci.* **2023**, *24*, 1344. [CrossRef]
89. Yang, A.C.; Vest, R.T.; Kern, F.; Lee, D.P.; Agam, M.; Maat, C.A.; Losada, P.M.; Chen, M.B.; Schaum, N.; Khoury, N.; et al. A human brain vascular atlas reveals diverse mediators of Alzheimer's risk. *Nature* **2022**, *603*, 885–892. [CrossRef]
90. Veys, K.; Fan, Z.; Ghobrial, M.; Bouché, A.; García-Caballero, M.; Vriens, K.; Conchinha, N.V.; Seuwen, A.; Schlegel, F.; Gorski, T.; et al. Role of the GLUT1 Glucose Transporter in Postnatal CNS Angiogenesis and Blood-Brain Barrier Integrity. *Circ. Res.* **2020**, *127*, 466–482. [CrossRef]
91. Denninger, J.K.; Walker, L.A.; Chen, X.; Turkoglu, A.; Pan, A.; Tapp, Z.; Senthilvelan, S.; Rindani, R.; Kokiko-Cochran, O.N.; Bundschuh, R.; et al. Robust Transcriptional Profiling and Identification of Differentially Expressed Genes With Low Input RNA Sequencing of Adult Hippocampal Neural Stem and Progenitor Populations. *Front. Mol. Neurosci.* **2022**, *15*, 810722. [CrossRef]
92. Finak, G.; McDavid, A.; Yajima, M.; Deng, J.; Gersuk, V.; Shalek, A.K.; Slichter, C.K.; Miller, H.W.; McElrath, M.J.; Prlic, M.; et al. MAST: A flexible statistical framework for assessing transcriptional changes and characterizing heterogeneity in single-cell RNA sequencing data. *Genome Biol.* **2015**, *16*, 278. [CrossRef] [PubMed]
93. Sherman, B.T.; Hao, M.; Qiu, J.; Jiao, X.; Baseler, M.W.; Lane, H.C.; Imamichi, T.; Chang, W. DAVID: A web server for functional enrichment analysis and functional annotation of gene lists (2021 update). *Nucleic Acids Res.* **2022**, *50*, W216–W221. [CrossRef]
94. Wu, T.; Hu, E.; Xu, S.; Chen, M.; Guo, P.; Dai, Z.; Feng, T.; Zhou, L.; Tang, W.; Zhan, L.; et al. clusterProfiler 4.0: A universal enrichment tool for interpreting omics data. *Innovation* **2021**, *2*, 100141. [CrossRef] [PubMed]
95. Tang, D.; Chen, M.; Huang, X.; Zhang, G.; Zeng, L.; Wu, S.; Wang, Y. SRplot: A free online platform for data visualization and graphing. *PLoS ONE* **2023**, *18*, e0294236. [CrossRef] [PubMed]